

# ISVR Technical Memorandum

## SCIENTIFIC PUBLICATIONS BY THE ISVR

*Technical Reports* are published to promote timely dissemination of research results by ISVR personnel. This medium permits more detailed presentation than is usually acceptable for scientific journals. Responsibility for both the content and any opinions expressed rests entirely with the author(s).

*Technical Memoranda* are produced to enable the early or preliminary release of information by ISVR personnel where such release is deemed to be appropriate. Information contained in these memoranda may be incomplete, or form part of a continuing programme; this should be borne in mind when using or quoting from these documents.

*Contract Reports* are produced to record the results of scientific work carried out for sponsors, under contract. The ISVR treats these reports as confidential to sponsors and does not make them available for general circulation. Individual sponsors may, however, authorize subsequent release of the material.

### COPYRIGHT NOTICE

(c) ISVR University of Southampton All rights reserved.

ISVR authorises you to view and download the Materials at this Web site ("Site") only for your personal, non-commercial use. This authorization is not a transfer of title in the Materials and copies of the Materials and is subject to the following restrictions: 1) you must retain, on all copies of the Materials downloaded, all copyright and other proprietary notices contained in the Materials; 2) you may not modify the Materials in any way or reproduce or publicly display, perform, or distribute or otherwise use them for any public or commercial purpose; and 3) you must not transfer the Materials to any other person unless you give them notice of, and they agree to accept, the obligations arising under these terms and conditions of use. You agree to abide by all additional restrictions displayed on the Site as it may be updated from time to time. This Site, including all Materials, is protected by worldwide copyright laws and treaty provisions. You agree to comply with all copyright laws worldwide in your use of this Site and to prevent any unauthorised copying of the Materials.

UNIVERSITY OF SOUTHAMPTON  
INSTITUTE OF SOUND AND VIBRATION RESEARCH  
DYNAMICS GROUP

**Investigation of the Mechanical and Electrical Properties of Actuators  
for Active Vibration Isolation**

by

**W. Fakkaew and M.J. Brennan**

ISVR Technical Memorandum No: 989

September 2010

Authorised for issue by  
Professor Brian Mace  
Group Chairman

## **Acknowledgements**

The first author would like to acknowledge financial support by the Thailand Research Fund through the Royal Golden Jubilee Ph.D. Program (Grant No. PHD/0227/2550).

# Contents

Acknowledgements	ii
Contents	iii
List of figures	iv
List of tables	vii
Abstract	viii
<b>1. Introduction</b>	<b>1</b>
<b>2. General model of actuator</b>	<b>3</b>
2.1 Electromagnetic actuator	3
2.2 Magnetostrictive actuator	6
2.3 Piezoelectric stack actuator	9
<b>3. Actuator identification</b>	<b>11</b>
3.1 Test rig design	11
3.2 Model parameter identification	13
3.3 Experimental work	16
<b>4. Comparison of the actuators</b>	<b>24</b>
<b>5. Application in active vibration isolation system</b>	<b>31</b>
5.1 Stability consideration	31
5.2 Active control demonstration	35
<b>6. Summary</b>	<b>48</b>
<b>7. References</b>	<b>50</b>

## List of figures

<b>Figure 1.</b> Lorentz force principle (a) a current carrying conductor in a magnetic field (b) a conductor moves through a magnetic field	4
<b>Figure 2.</b> Schematic diagram of an electromagnetic actuator	4
<b>Figure 3.</b> The equivalent (a) conventional diagram and (b) electrical circuit of the linear actuator	5
<b>Figure 4.</b> Relationship between (a) the magnetic field $H$ and the magnetization $M$ and (b) the magnetic field $H$ and mechanical strain $\epsilon$	6
<b>Figure 5.</b> Schematic diagram of magnetostrictive actuator	7
<b>Figure 6.</b> Diagram showing the superposition method of deriving the constitutive equation	7
<b>Figure 7.</b> Illustration of a piezoelectric stack actuator	10
<b>Figure 8.</b> Lay out of actuator identification set up	11
<b>Figure 9.</b> The equivalent (a) mobility diagram and (b) simplified mobility diagram	12
<b>Figure 10.</b> Frequency response functions of Eq. (26a) that have the same stiffness and damping but different mass, (a) Magnitude (b) Phase	15
<b>Figure 11.</b> Blocked force measurement set-up. The actuator connects to the block through the force gauge by (a) stinger 1 or (b) stinger 2. (c) Test circuit.	17
<b>Figure 12.</b> The measured blocked force per unit current of electromagnetic actuator model LDS V201 (a) Magnitude, (b) Phase	18
<b>Figure 13.</b> The measured electrical impedance of the electromagnetic actuator (a) magnitude, (b) phase, (c) resistance, (d) inductance.	18
<b>Figure 14.</b> The experimental set-up for the electromagnetic actuator (a) without proof mass (b) with proof mass	20
<b>Figure 15.</b> The experimental set up for the magnetostrictive actuator (a) without proof mass (b) with proof mass	20
<b>Figure 16.</b> The experimental set up for the piezoelectric stack actuator (a) without proof mass (b) with proof mass	20
<b>Figure 17.</b> The electrical circuit of (a) electromagnetic actuator and magnetostrictive actuator and (b) piezoelectric actuator	21

<b>Figure 18.</b> Experimental result of electromagnetic actuator (i) without and (ii) with proof mass, (a)–(b) The magnitude and phase of acceleration per unit input current and (c)–(d) the magnitude and phase of voltage across the actuator per unit current	22
<b>Figure 19.</b> Experimental result of magnetostrictive actuator (i) without and (ii) with proof mass, (a)–(b) The magnitude and phase of acceleration per unit input current and (c)–(d) the magnitude and phase of voltage across the actuator per unit input current	23
<b>Figure 20.</b> Experimental result of piezoelectric stack actuator (i) without and (ii) with proof mass, (a)–(b) The magnitude and phase of acceleration per unit input voltage and (c)–(d) the magnitude and phase of current per unit input voltage	23
<b>Figure 21.</b> Mobility diagram for power transmission consideration	28
<b>Figure 22.</b> (a) Force against displacement, (b) Square of modulus of free displacement per unit input electrical power, (c) square of the modulus of the block force per unit input electrical power, (d) Maximum efficiency of the actuators	29
<b>Figure 23.</b> Element of the robust control problem	32
<b>Figure 24.</b> Uncertainty and weighting transfer function of the electromagnetic actuator and magnetostrictive actuators.	36
<b>Figure 25.</b> (a) Current driver and (b) Voltage driver	37
<b>Figure 26.</b> Block diagram of the actuator when it is driven by (a) current driven or (b) voltage driver	37
<b>Figure 27.</b> Single axis active vibration isolation system using (a) soft-actuator and (b) stiff-actuator	38
<b>Figure 28.</b> Root locus of <i>system 1</i> (the right hand side picture zooms in the locus near the origin)	40
<b>Figure 29.</b> Root locus of <i>system 2</i> (two below pictures zoom in the locus near the origin)	41
<b>Figure 30.</b> Robust stability and robust performance plot of <i>system 1</i> using gain $g = 150, 600, 2400$ (arrows indicate the direction of increasing gain)	42
<b>Figure 31.</b> Robust stability and robust performance plot of <i>system 2</i> using gain $g = 500, 2000, 8000$ (arrows indicate the direction of increasing gain)	42

<b>Figure 32.</b> Robust stability and robust performance plot of the <i>system 1</i> and <i>system 2</i>	42
<b>Figure 33.</b> Root locus of <i>system 3</i>	45
<b>Figure 34.</b> Root locus of the system 4	45
<b>Figure 35.</b> Root locus of <i>system 3</i> with external damper	46
<b>Figure 36.</b> Root locus of <i>system 4</i> with external damper	46
<b>Figure 37.</b> Robust stability and robust performance plot of <i>system 3</i> using gain $k = 4000, 16\ 000, 64\ 000$ (arrows indicate the direction of increasing gain)	47
<b>Figure 38.</b> Robust stability and robust performance plot of <i>system 4</i> using gain $k = 25\ 000, 100\ 000, 400\ 000$ (arrows indicate the direction of increasing gain)	47
<b>Figure 39.</b> Robust stability and robust performance plot of the <i>system 3</i> and <i>system 4</i>	47

## List of tables

<b>Table 1.</b> Typical properties of actuators	16
<b>Table 2.</b> The mechanical and electrical properties of each actuator obtained from the experiment.	22
<b>Table 3.</b> The important parameters and equations for each actuator	29

## **Abstract**

In this report, the mechanical and electrical properties of three types of actuators are investigated. The actuators of interest are electromagnetic, magnetostrictive and piezoelectric. The constitutive equation of each actuator is presented in the form of a two-port model. The models are validated by comparing numerical simulation results with experimental data. A demonstration of controller design for active vibration isolation system using an electromagnetic actuator and a magnetostrictive actuator are also presented. The effects of using a current driver or a voltage driver with the actuator are discussed.

## 1. Introduction

Active vibration isolation systems are applied in many areas such as automobile, semiconductor manufacturing, biomedical engineering and aerospace engineering. However, the requirements of the actuator for each application may be different. In order to achieve good performance, the characteristics and the limitations of the actuator should be known in the controller design process. There are several mechanisms in general use in active vibration control systems, such as variable reluctance, moving coil electromagnetic, magnetostrictive, and piezoelectric, etc. Electromagnetic actuators have been used for many years in vibration control and testing. They are generally linear and relatively cheap, but their force generation per unit weight and volume is quite small. Magnetostrictive and piezoelectric actuators are generally more compact and can generate larger forces compared to their size [1].

The studies of actuator characteristics are usually based on both theoretical and experimental study. The objective of most studies is to model the actuator especially the hysteresis of piezoelectric and magnetostrictive actuators in order to improve the accuracy in position control [2,3,4]. Brennan et al [1], have studied different technologies for active vibration control based on an experimental investigation. The mechanical and electrical properties were described by using a two-port system model effectively.

An accurate nonlinear model might be important for position or velocity control, but it is not necessarily important in vibration isolation problem. This is because the purpose of control is to suppress the payload displacement by stopping the vibrational energy from any disturbance source from reaching the payload. A linear two-port model can be used to describe the behaviour of the actuators that are used in vibration isolation, and the model error can be treated as unstructured uncertainty. When the system is subjected to the uncertainty, the problem becomes a robust control problem in which knowledge of an uncertainty bound is necessary, as it concerns the stability of the system. A large uncertainty can degrade the performance of the system [5]. The

uncertainty can be reduced by selecting linear hardware and using the suitable model to describe the system.

In this study, three types of actuator are modelled including an electromagnetic actuator, a magnetostrictive actuator and a piezoelectric actuator. The two-port model is used to describe the actuators, and the uncertainty bound of each element of the two-port system is also identified. Following this introduction, the report is organized into five sections. The first part of this report introduces an operational principle and a constitutive equation (the two-port model) for each actuator. Next, the parameter identification method and identification results are presented. Then, the mechanical and electrical properties of each actuator that can be used in actuator selection are compared. After that, the effect of uncertainties due to identification errors on active the vibration isolation stability and performance is demonstrated. Finally, all results are summarized and discussed in the last section.

## 2. General model of actuator

An actuator is an item of equipment that converts electrical energy to mechanical energy. It can be viewed as a two-port model relating the electrical properties at one port to the mechanical properties at the other. Assuming linearity, the relation between the mechanical and electrical parameter is given by [6]

$$\begin{Bmatrix} f \\ v \end{Bmatrix} = \begin{bmatrix} Z_m & T_1 \\ T_2 & Z_e \end{bmatrix} \begin{Bmatrix} u \\ i \end{Bmatrix} \quad (1a)$$

$$\quad (1b)$$

or

$$\begin{Bmatrix} u \\ i \end{Bmatrix} = \begin{bmatrix} (Z_m)^{-1} & T_1^i \\ T_2^i & (Z_e)^{-1} \end{bmatrix} \begin{Bmatrix} f \\ v \end{Bmatrix} \quad (2a)$$

$$\quad (2b)$$

where  $f$ ,  $u$ ,  $v$  and  $i$  are force, relative velocity, voltage and current respectively.  $Z_m$  and  $Z_e$  are mechanical impedance and electrical impedance respectively and  $T_1$

and  $T_2$  are actuator constant,  $Z_m^i = Z_m \left(1 - \frac{T_1 T_2}{Z_m Z_e}\right)$ ,  $Z_e^i = Z_e \left(1 - \frac{T_1 T_2}{Z_m Z_e}\right)$ ,  $T_1^i = T_1 \left(1 - \frac{Z_m Z_e}{T_1 T_2}\right)$  and  $T_2^i = T_2 \left(1 - \frac{Z_m Z_e}{T_1 T_2}\right)$ . In general,  $|T_1| = |T_2|$  and the

sign of actuator constants depend on actuator design, e.g., if positive current causes positive displacement, the sign of  $T_1$  is minus and vice versa. When the actuator is constrained not to move,  $u = 0$ , the force that the actuator generates,  $f_B$ , is called *blocked force*. On the other hand, the displacement that is generated by an unconstrained actuator,  $f = 0$ , is called *free displacement*.

### 2.1 Electromagnetic actuator

Electromagnetic actuator operates on the Lorentz's principle. If a current carrying conductor is placed in a magnetic field, there will be a force exerted upon it as shown in figure 1. The force can be determined by

$$\mathbf{F} = \mathbf{I} \times \mathbf{B}. \quad (3)$$

where bold font denote a vector,  $\mathbf{F}$  is Lorentz force (N),  $\mathbf{I}$  is current flow in the conductor (A),  $\mathbf{B}$  is magnetic flux density and  $l$  is the conductor length.

Conversely, if the conductor moves through a magnetic field vector  $\mathbf{B}$  with the velocity  $\mathbf{u}$ , the voltage  $\mathbf{E}$  will be induced across the conductor that can be expressed by

$$\mathbf{E} = \mathbf{u} \times \mathbf{B}. \quad (4)$$

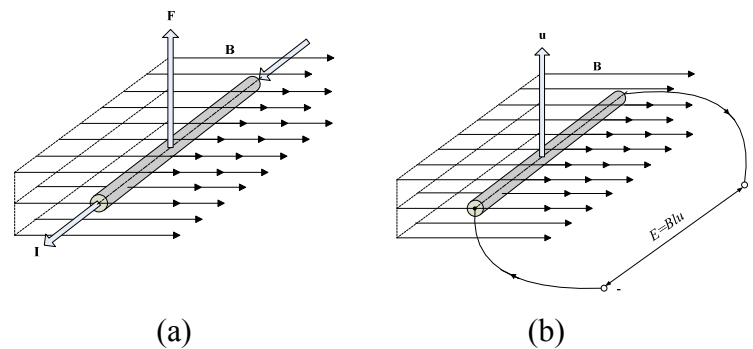


**Figure 1.** Lorentz force principle (a) a current carrying conductor in a magnetic field (b) a conductor moves through a magnetic field

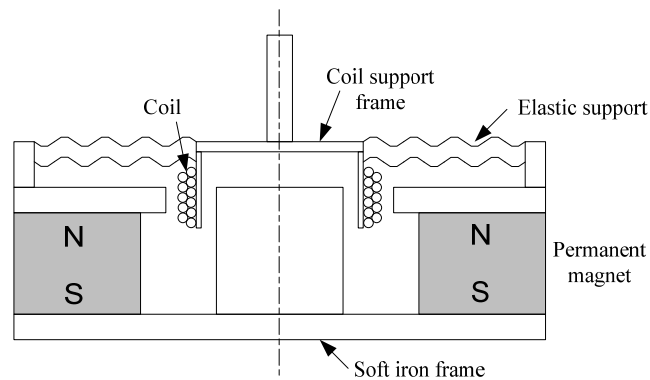


**Figure 2.** Schematic diagram of an electromagnetic actuator

A schematic diagram of the electromagnetic actuator is shown in figure 2. The coil of wire is held in a permanent magnetic field by the flexible suspension that is modelled by a spring and damper element. The equivalent conventional diagram and electrical circuit diagram of the actuator is shown in figure 3. Assuming positive current gives positive displacement, the equation of motion of the moving element and the current-voltage relation (in frequency domain) can be written by

$$F_A - m_2(j\omega U_A) = c(U_A - U_B) + k\left(\frac{U_A}{j\omega} - \frac{U_B}{j\omega}\right) - Bli$$

$$F_B - m_2(j\omega U_B) = -c(U_A - U_B) - k\left(\frac{U_A}{j\omega} - \frac{U_B}{j\omega}\right) + Bli$$

$$-V + Ri + L(j\omega I) + Bl(U_A - U_B) = 0$$

or equivalently

$$\begin{Bmatrix} F_A \\ F_B \\ V \end{Bmatrix} = \begin{bmatrix} j\omega m_1 + c + \frac{k}{j\omega} & -\left(c + \frac{k}{j\omega}\right) & -Bl \\ \left(c + \frac{k}{j\omega}\right) & j\omega m_2 + c + \frac{k}{j\omega} & Bl \\ Bl & -Bl & R + j\omega L \end{bmatrix} \begin{Bmatrix} U_A \\ U_B \\ I \end{Bmatrix}$$

where  $m_1$  is mass of moving element and  $m_2$  is mass of actuator case.

Assuming  $U_A - U_B \approx U_A$ , it can be simplified to

$$\begin{Bmatrix} F \\ V \end{Bmatrix} = \begin{bmatrix} j\omega m_1 + c + \frac{k}{j\omega} & -Bl \\ Bl & R + j\omega L \end{bmatrix} \begin{Bmatrix} U_A \\ I \end{Bmatrix} \quad (5)$$

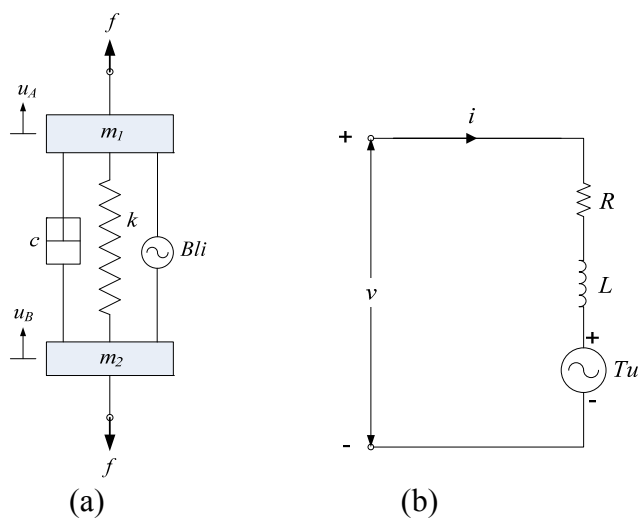


**Figure 3.** The equivalent (a) conventional diagram and (b) electrical circuit of the linear actuator

## 2.2 Magnetostrictive actuator

Magnetostriction is the phenomenon that the shape of certain materials changes when the materials are subject to a magnetic field. Conversely, the magnetization changes when the materials are subject to a mechanical stress. This phenomena can be used for actuation and sensing. The nature of the magnetic and mechanical phenomena are usually illustrated as in figure 4 [4,7]. The relationship between the magnetic field  $H$  and the magnetization  $M$  is nonlinear due to hysteresis. The relationship between the magnetic field  $H$  and the strain  $\epsilon$  is also nonlinear and has the shape of a butterfly curve. As a result, a bias magnetic field and pre-stress is required to improve the characteristics of the actuator. Figure 5 shows a schematic diagram of a commercial magnetostrictive actuator [4]. The disc spring is employed to provide a compact compressional pre-stress. The magnetic bias field is generated by the permanent magnet. A solenoid coil wound around the drive rod to either add or subtract from the existing bias magnetic field, causes the drive rod to either expand or contract in response.

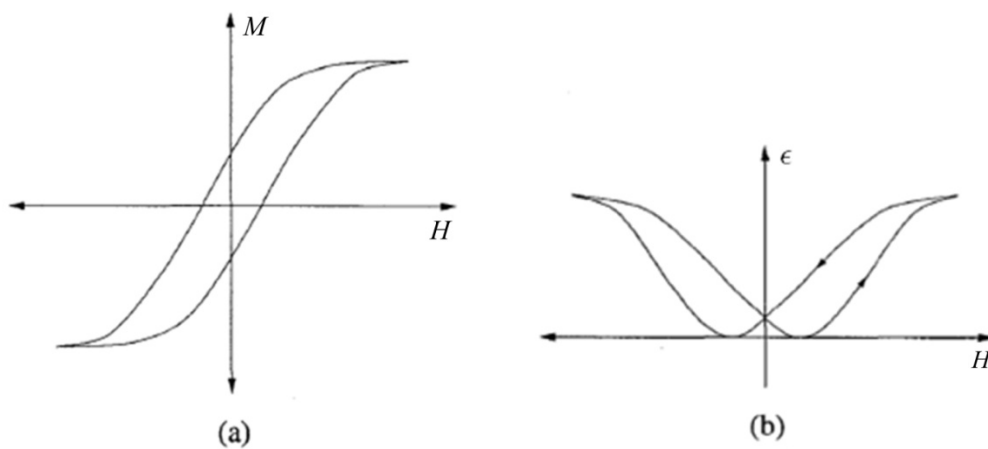


**Figure 4.** Relationship between (a) the magnetic field  $H$  and the magnetization  $M$  and (b) the magnetic field  $H$  and mechanical strain  $\epsilon$

To model the magnetostrictive actuator, a starting point is the linear constitutive equation as follows [7]:

$$\epsilon = \frac{1}{Y}\sigma + \alpha h \quad (6)$$

$$b = \alpha\sigma + \mu h$$

where  $Y$  is Young's modulus,  $\mu$  is Permeability,  $\alpha$  is magnetostrictive constant,  $\epsilon$  is strain,  $\sigma$  is stress,  $b$  is magnetic flux density and  $h$  is magnetic field strength.

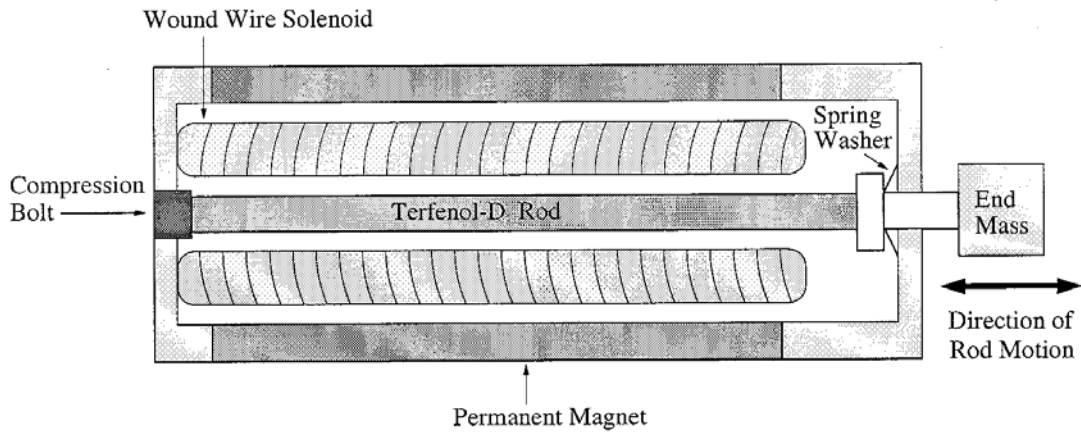


**Figure 5.** Schematic diagram of magnetostrictive actuator [4]

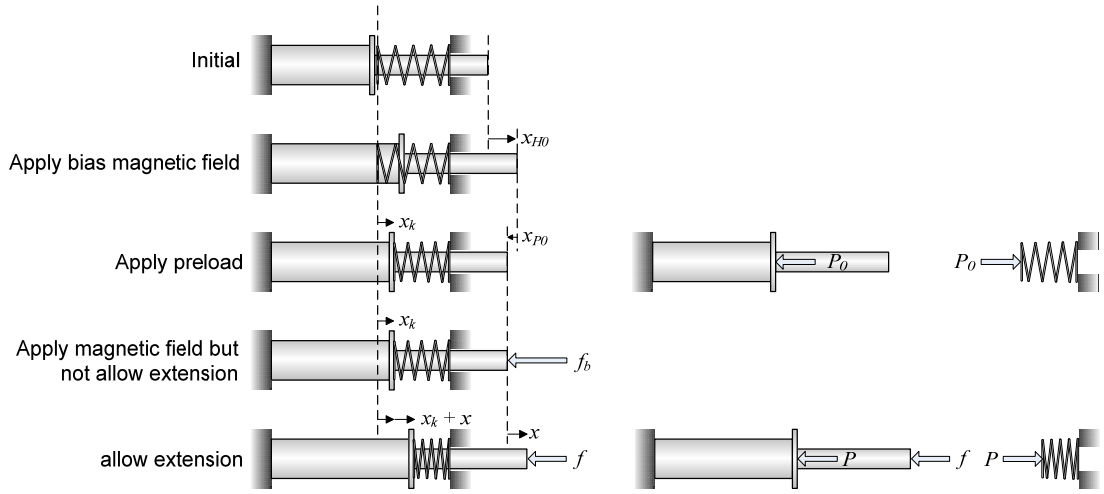


**Figure 6.** Diagram showing the superposition method of deriving the constitutive equation

Consider figure 6 that shows the superposition method for deriving the constitutive equation of magnetostrictive actuator. After applying the bias magnetic field  $H_0$  and preload  $P_0 = k_p x_k$ , the constitutive Eq. (6) becomes

$$\frac{x_{H_0} - x_{P_0}}{l} = \frac{1}{Y} \frac{k_p x_k}{A} + \alpha H_0 \quad (7)$$

$$B_0 = \alpha \frac{k_p x_k}{A} + \mu H_0$$

where  $k_p$  is the stiffness of preload spring,  $A$  is the cross-sectional area and  $l$  is an effective length. If the magnetic field  $h$  is generated by exciting solenoid coil with a certain current causing the extension  $x$  and force  $f$  acting at the end of the rod, the constitutive Eq. (6) becomes

$$\frac{x}{l} + \frac{x_{H_0} - x_{P_0}}{l} = \frac{1}{Y} \left( \frac{k_p x_k}{A} + \frac{f}{A} \right) + \alpha (H_0 + h)$$

$$b + B_0 = \alpha \left( \frac{k_p x_k}{A} + \frac{f}{A} \right) + \mu (H_0 + h)$$

Equation (7) still holds so that

$$\frac{x}{l} = \frac{1}{YA} f + \alpha h \quad (8a)$$

$$b = \alpha \frac{f}{A} + \mu h \quad (8b)$$

or equivalently

$$f = \frac{YA}{l}x - \alpha YAh \quad (9a)$$

$$b = \frac{\alpha Y}{l}x + (\mu - \alpha^2 Y)h. \quad (9b)$$

Since  $v = NA \frac{db}{dt}$ , substituting  $h = \frac{Nl}{\mu}$  in Eq. (9), pre-multiplying Eq. (9b) by  $NA$  and differentiating (9b) with respect to time, gives

$$f = \frac{YA}{l}x - \frac{\alpha YAN}{l}l \quad (10a)$$

$$v = \frac{\alpha YAN}{l}u + \frac{(\mu - \alpha^2 Y)AN^2}{l} \frac{dl}{dt}. \quad (10b)$$

where  $u = \frac{dx}{dt}$  is the relative velocity. Now,  $\frac{YA}{l}$  is the stiffness of the magnetostrictive

rod,  $\frac{\mu AN^2}{l}$  is the inductance of the solenoid coil and  $\frac{\alpha YAN}{l}$  is the actuator constant.

Given  $k = \frac{YA}{l}$ ,  $L_s = \frac{(\mu - Yd^2)AN^2}{l}$  and  $T = \frac{\alpha YAN}{l}$  then Eq. (10) becomes

$$f = kx - Tl \quad (11a)$$

$$v = Tu + L_s \frac{dl}{dt}. \quad (11b)$$

Note that the hysteresis effects in the magnetostrictive rod and the solenoid coil are not included in Eq. (11). In the frequency domain the linear constitutive equation that includes the hysteresis effect and effective rod mass can be represented by

$$\begin{Bmatrix} F \\ V \end{Bmatrix} = \begin{bmatrix} j\omega m_1 + c + \frac{k}{j\omega} & -T \\ T & R + j\omega L_s \end{bmatrix} \begin{Bmatrix} U_A \\ l \end{Bmatrix} \quad (12)$$

where  $c$  is equivalent damping constant.

### 2.3 Piezoelectric stack actuator

Piezoelectric ceramics transform energy between the electrical and mechanical domains. Application of an electric field across the ceramic creates a mechanical strain, and in a similar manner, application of a mechanical stress to the ceramic

induces an electrical charge. The fundamental component of a piezoelectric stack actuator is a wafer of piezoelectric material sandwiched between two electrodes as shown in figure 7. One dimensional linear constitutive equations describing the piezoelectric effect are given by [2]

$$\begin{aligned} \epsilon &= \frac{1}{Y}\sigma + \beta e \\ d &= \beta\sigma + \epsilon e \end{aligned} \quad (13)$$

where  $Y$  is Young's modulus,  $\epsilon$  is permittivity,  $\beta$  is piezoelectric constant,  $\epsilon$  is strain,  $\sigma$  is stress,  $e$  is electric field and  $d$  is dielectric displacement.

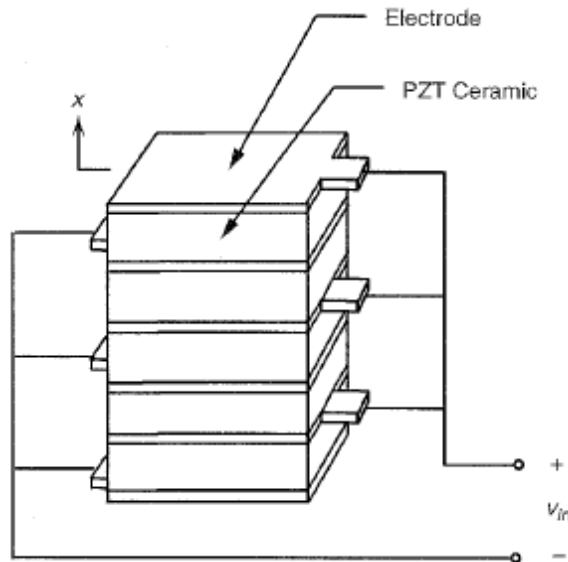


**Figure 7.** Illustration of a piezoelectric stack actuator

The variables,  $\epsilon = \frac{x}{l}$ ,  $\sigma = \frac{f}{A}$ ,  $e = \frac{v}{L}$  and  $d = \frac{q}{A}$  where  $n$  is number of elements in the stack can be substituted into Eq. (13) to give

$$\begin{aligned} x &= \frac{l}{YA}f + n\beta v \\ q &= n\beta f + \frac{n^2\epsilon A}{l} v \end{aligned}$$

or equivalently

$$f = \frac{YA}{l}x - \frac{n\beta YA}{l}v \quad (14a)$$

$$q = \frac{n\beta YA}{l}x + \left( \frac{n^2sA}{l} - \frac{n^2\beta^2YA}{l} \right)v \quad (14b)$$

Differentiating these two equations respect with time, and substituting  $\frac{dx}{dt} = u$ ,  $\frac{dq}{dt} = \dot{v}$ ,  $\frac{YA}{L} = k$ ,  $\frac{n^2sA}{L} - \frac{n^2\beta^2YA}{l} = C_\varphi$  and  $\frac{n\beta YA}{l} = T'$ , results in

$$\begin{aligned} f &= kx - T'v \\ \dot{v} &= T'u + C_\varphi \dot{v} \end{aligned} \quad (15)$$

The hysteresis effect in the piezoelectric stack is not included in Eq. (15). In the frequency domain the linear constitutive equation that includes the hysteresis effect and the effective mass of the rod can be represented by

$$\begin{Bmatrix} F \\ l \end{Bmatrix} = \begin{bmatrix} j\omega m_1 + c + \frac{k}{j\omega} & -T' \\ T' & \left( R + \frac{1}{j\omega C_\varphi} \right)^{-1} \end{bmatrix} \begin{Bmatrix} U_A \\ v \end{Bmatrix}. \quad (16)$$

where  $c$  is equivalent damping constant.

### 3. Actuator identification

This section concerns the identification of the actuator parameters. For simplicity it is assumed that the actuator is a single axis actuator. Since it is assumed that  $U_A - U_B \approx U_A$ , the condition for this assumption to hold is discussed as is the resulting design of the experimental set-up.

#### 3.1 Test rig design

Consider the system shown in figure 8, which depicts the actuator under test placed between two spring-mass-damper sub-systems. The masses of the moving element and actuator case of the actuator are modelled as lumped masses and are depicted by  $m_1$  and  $m_2$  respectively.

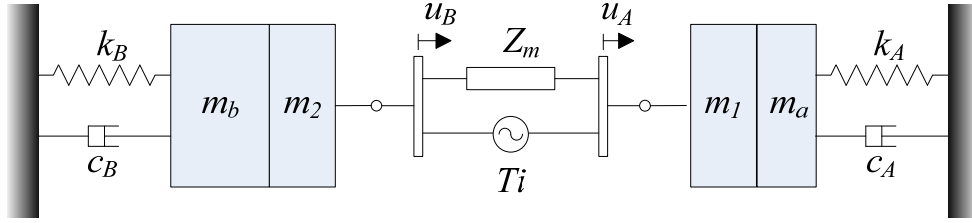


**Figure 8.** Lay out of actuator identification set-up

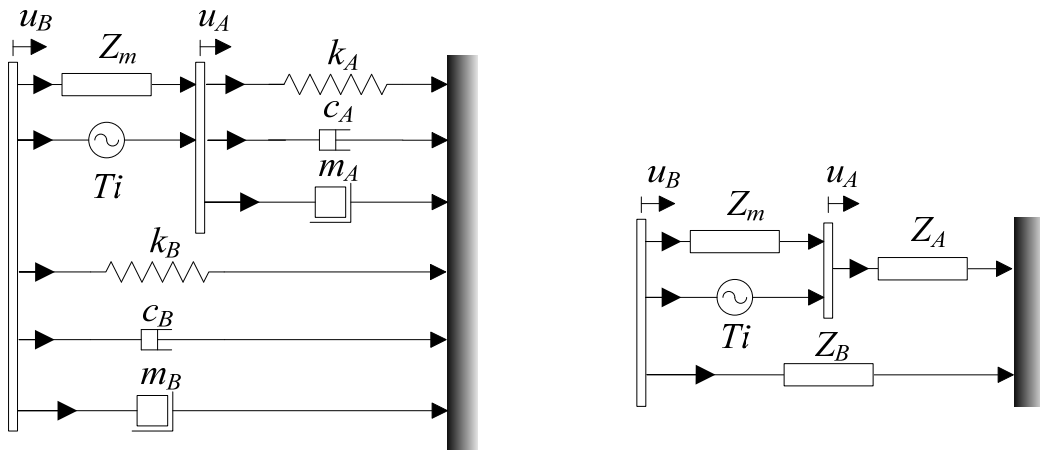
The equivalent mobility diagram and simplified mobility diagram are shown in figure 9 where  $m_A = m_1 + m_a$  and  $m_B = m_2 + m_b$ . If the actuator is excited by the sinusoidal current  $i = I e^{j\omega t}$  where  $j = \sqrt{-1}$  and  $\omega$  is the angular velocity, the response of the system is assumed to be  $\begin{Bmatrix} u_A \\ u_B \end{Bmatrix} = \begin{Bmatrix} U_A \\ U_B \end{Bmatrix} e^{j\omega t}$ . Applying Kirchoff's law to the system shown in figure 9b, results in

$$\begin{bmatrix} Z_m + Z_A & Z_m \\ -Z_m & Z_m + Z_B \end{bmatrix} \begin{Bmatrix} U_A \\ U_B \end{Bmatrix} = \begin{bmatrix} T \\ -T \end{bmatrix} I \quad (17)$$

where

$$Z_A = j\omega m_A + c_A + \frac{k_A}{j\omega} \quad (18)$$

$$Z_B = j\omega m_B + c_B + \frac{k_B}{j\omega}. \quad (19)$$



(a)

(b)

**Figure 9.** The equivalent (a) mobility diagram and (b) simplified mobility diagram

Solving Eq. (17) and rearranging the result gives

$$U_A = \frac{T}{Z_A + Z_m \left(1 + \frac{Z_A}{Z_B}\right)} I \quad (20)$$

$$U_B = \frac{-\frac{Z_A}{Z_B} T}{Z_A + Z_m \left(1 + \frac{Z_A}{Z_B}\right)} I. \quad (21)$$

Equations (20) and (21) combine to give

$$\frac{U_B}{U_A} = \frac{Z_A}{Z_B} = \frac{m_A}{m_B} \left( \frac{-\omega^2 + j\omega \frac{c_A}{m_A} + \frac{k_A}{m_A}}{-\omega^2 + j\omega \frac{c_B}{m_B} + \frac{k_B}{m_B}} \right) = \gamma(j\omega) \quad (22)$$

Since

$$U_B - U_A = -U_A(1 - \gamma(j\omega)) \quad (23)$$

$$U_B - U_A \approx -U_A \text{ if } \gamma(j\omega) \ll 1, \text{ that is } \frac{m_A}{m_B} \ll 1.$$

### 3.2 Model parameter identification

In the frequency domain, the constitutive Eq. (1) is given by

$$F = Z_m(U_A - U_B) + TI \quad (24a)$$

$$V = T(U_A - U_B) + Z_g I. \quad (24b)$$

where  $F$  and  $V$  are force and voltage amplitude of each frequency.

It is assumed that  $m_A/m_B \ll 1$  such that  $U_B - U_A \approx U_A$  and it is also assumed that  $k_A, c_A$  are equal to zero. Substitute  $F = -m_A(j\omega U_A)$  in (24a), then gives

$$\begin{aligned} -j\omega m_A U_A &= Z_m U_A + T I \\ V - T U_A + Z_s I & \end{aligned}$$

that is

$$\begin{aligned} \frac{U_A}{I} &= \frac{-T}{j\omega m_A + Z_m} \\ \frac{V}{I} &= Z_s + T \frac{U_A}{I} \end{aligned}$$

or

$$\frac{A_A}{I} = \frac{-j\omega T}{j\omega m_A + Z_m} \quad (25a)$$

$$\frac{V}{I} = Z_s + \frac{T A_A}{j\omega I} \quad (25b)$$

where  $A_A$  is the acceleration magnitude of mass  $m_A$ . Assuming  $Z_m = c + \frac{k}{j\omega}$ , and  $Z_s = R + j\omega L$ . Eq. (25) becomes

$$\frac{A_A}{I} = \frac{\omega^2 T_m}{-\omega^2 + j\omega(2\zeta\omega_n) + \omega_n^2} \quad (26a)$$

$$\frac{V}{I} = (R + j\omega L) + \frac{T A_A}{j\omega I} \quad (26b)$$

where  $\omega_n^2 = \frac{k}{m_A}$ ,  $2\zeta\omega_n = \frac{c}{m_A}$  and  $T_m = \frac{T}{m_A}$ . For the magnetostrictive actuator, it is assumed that  $Z_m = k(1 + j\eta)$  then Eq. (25) becomes

$$\frac{A_A}{I} = \frac{\omega^2 T_m}{-\omega^2 + j\omega(2\zeta\omega_n) + \omega_n^2} \quad (26c)$$

The piezoelectric actuator is a voltage driven device. If there is no external force  $F$  applied to the actuator, the constitutive Eq. (16) becomes

$$\frac{A_A}{V} = \frac{-\omega^2 T_m'}{-\omega^2 + j\omega(2\zeta\omega_n) + \omega_n^2} \quad (27a)$$

$$\frac{I}{V} = \left( R + \frac{1}{j\omega C_g} \right)^{-1} + \frac{T' A_A}{j\omega I} \quad (27b)$$

where  $\omega_n^2 = \frac{k}{m_A}$ ,  $2\zeta\omega_n = \frac{c}{m_A}$  and  $T'_m = \frac{T'}{m_A}$ .

To identify the model parameters, Eqs. (26a), (26c) or (27b) are plotted to compare the transfer function  $\frac{A_A}{I}$  or  $\frac{A_A}{V}$  that are obtained directly from the experiment. The parameters  $T'_m$  or  $T'_m$ ,  $\omega_n$ ,  $\zeta$  or  $\eta$  are assumed and are substituted into Eqs. (26a) or (26c) or (27a) by trial and error until they match with the experimental results. To determine  $m_1$  and  $k$  two experiments were set up using different values of  $m_a$ . Figure 10 shows the frequency response function of the two systems that have the same stiffness and damping but different mass. The stiffness  $k$  and mass  $m_1$  can be determined by

$$\begin{Bmatrix} k \\ m_1 \end{Bmatrix} = \begin{bmatrix} 1/\omega_1^2 & -1 \\ 1/\omega_2^2 & -1 \end{bmatrix}^{-1} \begin{Bmatrix} m_{a1} \\ m_{a2} \end{Bmatrix}. \quad (28)$$

where  $m_{a1}$  and  $m_{a2}$  are proof masses which are assumed to be known. The damping coefficient  $c$  is determined by

$$c = 2\zeta\omega_1 m_1. \quad (29)$$

and the actuator constant is obtained by

$$T = m_1 T'_m. \quad (30)$$

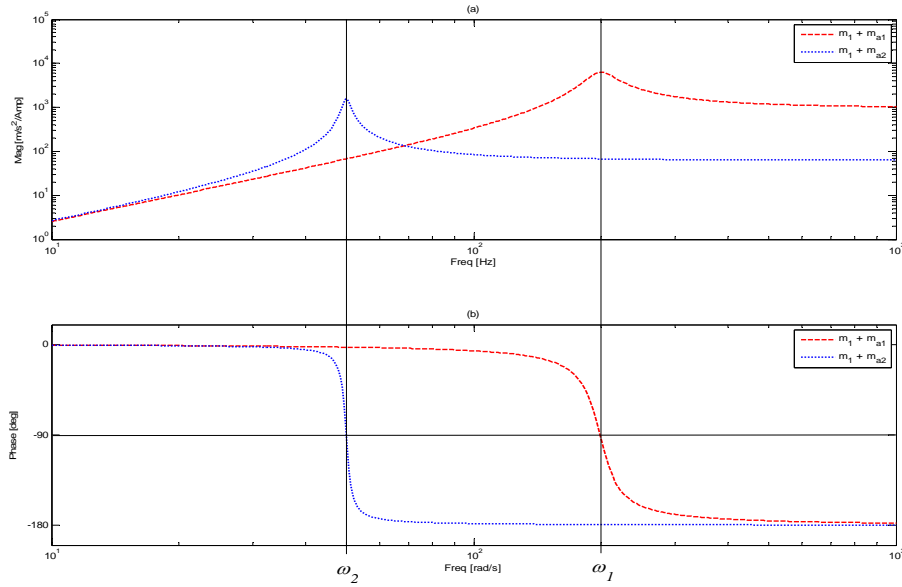


**Figure 10.** Frequency response functions of Eq. (26a) that have the same stiffness and damping but different mass, (a) Magnitude (b) Phase

To identify the electrical properties, Eqs. (26b), or (27b) are plotted to compare the

transfer functions  $\frac{V}{I}$  or  $\frac{I}{V}$  obtained directly from the experiment. The parameters  $T_m$  or  $T'_m$  are already known and  $R$ ,  $L$  or  $C_e$  are assumed and substituted into (26b) or (27b) by trial and error until it match well with the experimental results.

### 3.3 Experimental work

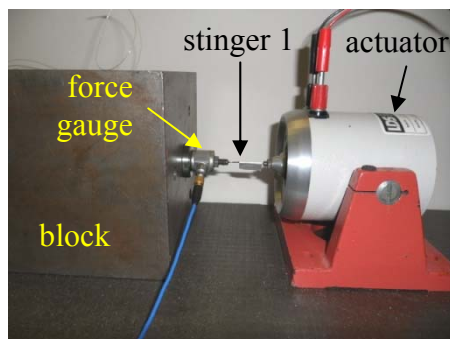
In this study, three types of actuators were available namely an electromagnetic actuator, a magnetostrictive actuator and a piezoelectric stack actuator. Their typical properties are shown in table 1. In the experiment, a *Data Physics*® signal analyzer model 70103 was used and the transfer function between the two signals could be obtained directly.

**Table 1.** Typical properties of actuators

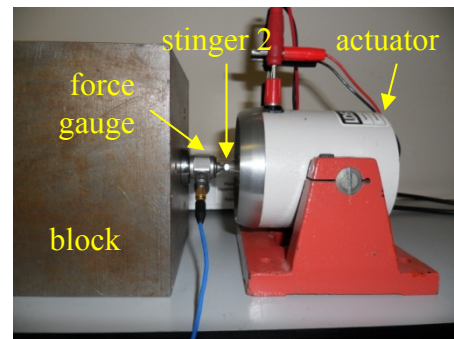
Property	Typical value		
	Electromagnetic LDS V201	Magnetostrictive Extrema AA-050H	Piezoelectric PI P840.60
1. Max. flocced force	± 26.7 N	± 462 N	1000 N (push) 50 N (pull)

2. Max. free displacement	$\pm 5 \text{ mm}$	$\pm 25 \text{ }\mu\text{m}$	$\pm 90 \text{ }\mu\text{m} \pm 20\%$
3. Max. input current (peak)	5 A	2 A	-
4. Max. input voltage (peak)	-	-	200 V
5. Armature resonance frequency	13000 Hz	6500 Hz	6 kHz $\pm 20\%$
6. Axial stiffness	8.76 N/mm	26.9 N/ $\mu\text{m}$	10 N/ $\mu\text{m} \pm 20\%$
7. Effective moving mass	0.020 kg	-	-
8. Resistance	-	3.2 $\Omega$	-
9. Inductance	-	2.1 mH	-
10. Capacitance	-	-	9 $\mu\text{F} \pm 20\%$

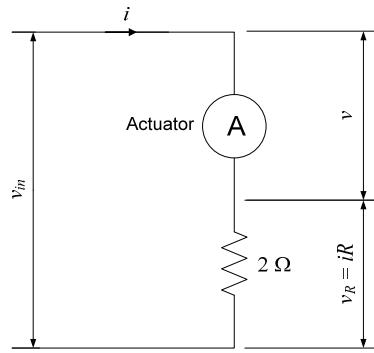
The magnetostrictive actuator and piezoelectric stack actuator are classified as stiff-actuators. It is difficult to measure the block force from this type of actuator because the deformation of the blocks they are attached to when the actuators are excited is quite large when compared with their free displacement. Therefore, it cannot be assumed that  $u = 0$ . However, it is possible to measure the blocked force of the soft-actuator such as an electromagnetic actuator because its free displacement is very large compared to the deformation of the blocks it is attached to. As a result, for the electromagnetic actuator, two different methods are employed to identify actuator constant and electrical impedance and the results are compared. The first experimental set up for the electromagnetic actuator is shown in figure 11. The actuator was excited by a random signal and the force  $f$  generated by actuator was measured by a piezoelectric force gauge of PCB™ model 208C01. The current  $i$  supplied was monitored by way of the voltage across a 2  $\Omega$  resistor in the supply line, and the voltage  $v$  across the actuator was also monitored.



(a)



(b)



(c)

**Figure 11.** Blocked force measurement set-up. The actuator connects to the block through the force gauge by (a) stinger 1 or (b) stinger 2. (c) Test circuit.

From the experimental set up, it was assumed that the velocity is equal to zero. From (5),

$$Bl = -\frac{F}{I} \quad (31)$$

and

$$R + j\omega L = \frac{V}{I}. \quad (32)$$

The blocked force per unit current from the experimental result is shown in figure 12.

In the low frequency range, the magnitude of  $\frac{F}{I}$  is constant which means that  $Bl = 5.4$  N/A and the phase difference is 180 degree. Theoretically, the measurement of  $\frac{F}{I}$  should be constant, however, the moving part of the actuator is not absolutely rigid so the resonance frequencies of two stingers that appear at 2113 Hz and 6513 Hz can be seen. The armature resonance frequency appears at 20 900 Hz and this is close to the typical value. The electrical impedance of the electromagnetic actuator is shown in figure 13a-b and the inductance and resistance are shown in figure 13c and 13d respectively. The resistance is 1.14  $\Omega$  in the low frequency range and increases with frequency. The inductance is approximately 0.46 mH and tends to decrease with frequency.

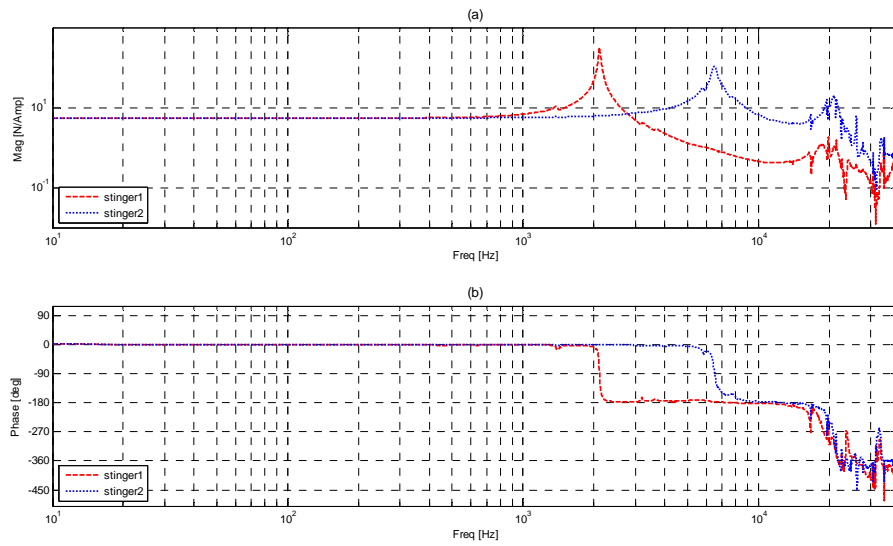


**Figure 12.** The measured blocked force per unit current of electromagnetic actuator model LDS V201 (a) Magnitude, (b) Phase

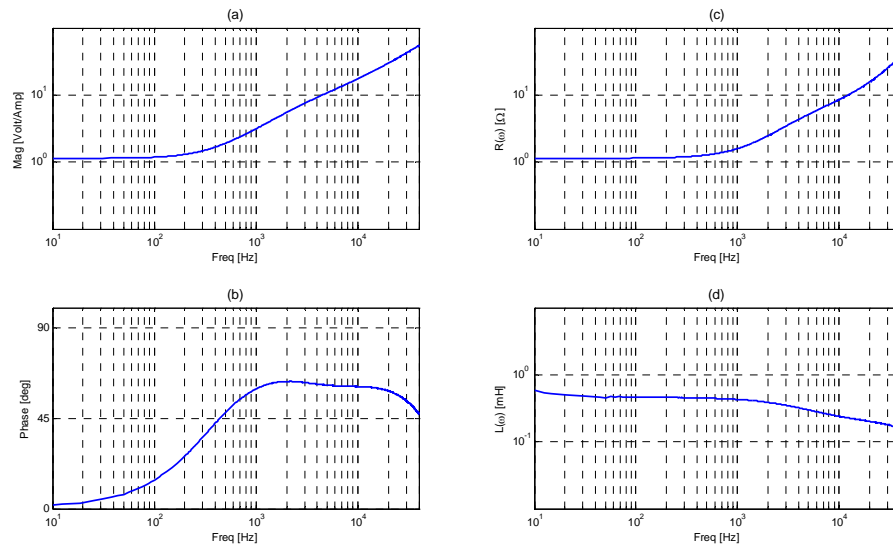


**Figure 13.** The measured electrical impedance of the electromagnetic actuator (a) magnitude, (b) phase, (c) resistance, (d) inductance.

In order to identify the parameters of each actuator following the procedure outlined in section 3.1, the experiment set up for each actuator is shown in figures 14-16. A proof mass  $m_a = 108.3$  g was used to identify the stiffness and the effective moving mass of the electromagnetic actuator. The mass ratio was

$$\frac{m_A}{m_B} \approx \frac{0.11}{3} \approx 0.037$$

which is considered small enough. The actuator was placed on the floor as shown in figure 14; the friction force was large enough to prevent the movement of the actuator case. The accelerometer was attached to the end of the moving part of the actuator to measure the acceleration. The accelerometer used in experiment is a piezoelectric accelerometer of PCB™ model 352C22. For the magnetostrictive actuator, the actuator was suspended by two strings as shown in figure 15 in order to set the support stiffness far below the actuator stiffness, and the external mass was added to the housing of the actuator to reduce the mass ratio. The proof mass was  $m_a = 11.6$  g and was used to identify the actuator, in this case, the

$$\text{mass ratio was } \frac{m_A}{m_B} \approx \frac{0.012}{0.450} \approx 0.033$$

. The acceleration of the moving part of the actuator was measured by the accelerometer. The current supplied to electromagnetic and magnetostrictive actuators was monitored by the measuring the voltage across the 2 Ω resistor that was connected in series with the actuator as shown in figure 17a. The voltage  $v$  across the actuator was monitored by direct measurement. For the piezoelectric stack actuator, it should be suspended but the piezoelectric stack inside the tube was broken so it was arranged in a vertical direction and a preload was applied on it. A proof mass of 7.7 g was used to identify the actuator, in this case, the mass ratio was not available because the mass  $m_B$  was unknown. The acceleration of the moving part of the actuator was measured by the accelerometer. The excitation voltage was available from the amplifier and the current flow through the actuator was measured by monitoring the voltage across the 1 Ω resistor that was connected in series with the actuator as shown in figure 17b. To obtain the transfer functions, the actuators were excited by random signals and acceleration, voltage and current were measured and passed to the signal analyzer. The transfer functions were obtained directly from the analyzer.

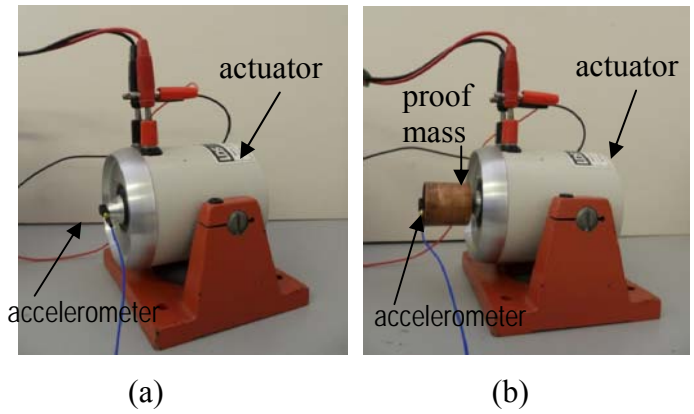


**Figure 14.** The experimental set-up for the electromagnetic actuator (a) without proof mass (b) with proof mass

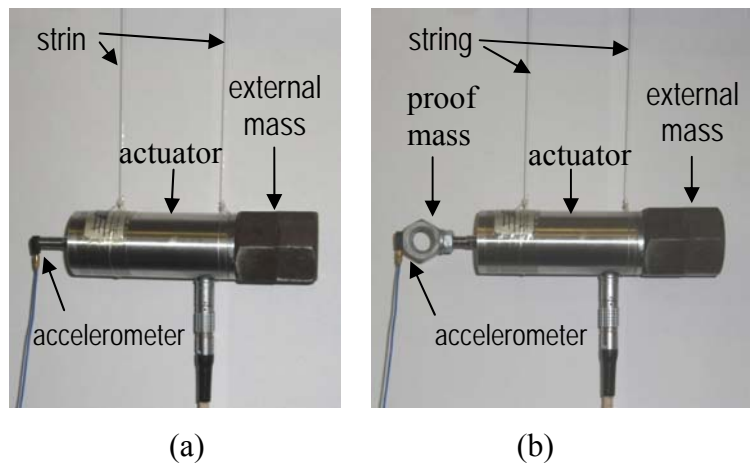


**Figure 15.** The experimental set up for the magnetostrictive actuator (a) without proof mass (b) with proof mass

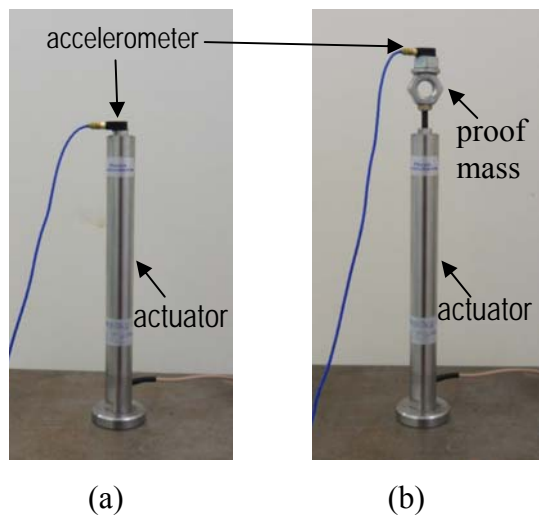


**Figure 16.** The experimental set up for the piezoelectric stack actuator (a) without proof mass (b) with proof mass

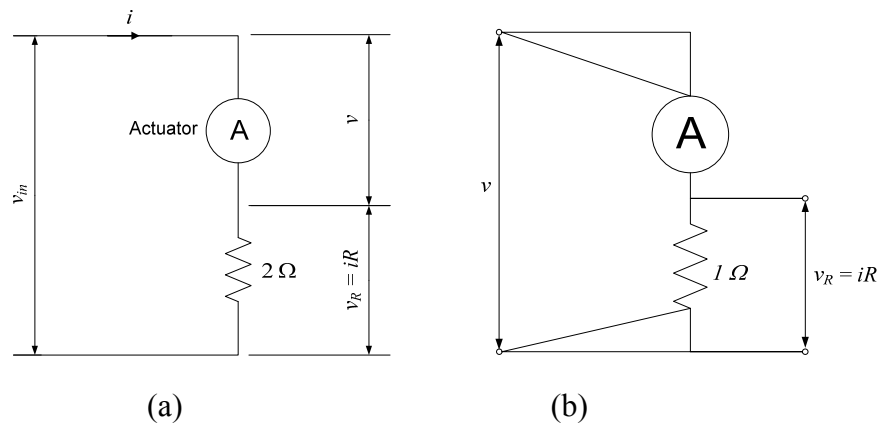


**Figure 17.** The electrical circuit of (a) the electromagnetic and magnetostrictive actuators and (b) the piezoelectric actuator

The experimental results are shown in figure 18–20. They show the magnitude and phase of acceleration per unit input current (or voltage) and voltage across the actuator per unit current of the actuator (or current per unit voltage) with and without a proof mass. A comparison is made with linear approximation models. The approximate linear model cannot predict the behaviour of the actuator correctly in the high frequency range because the actual actuators are multi-degree-of-freedom systems. However, the results show that the approximate linear model matches well with the experimental results in the low frequency range. As a result, the actuators can be considered to be a linear device if it is operated in the low frequency range. Using the procedure described in section 3.1, the model parameters for each actuator are shown in table 2. For the electromagnetic actuator, the actuator constant and electrical parameters obtained by two different methods are the same. For the magnetostrictive actuator, the resonance frequency is close to that given in the datasheet. The difference may be due to the measurement method, for example the mass of the accelerometer used may influence the resonance frequency because the effective moving mass is very small. The inductance of the actuator is similar to the typical value but the resistance is higher due to the additional contact resistance in the experimental set up. The first resonance frequency of the piezoelectric actuator is much lower than the typical value because the piezoelectric stack was broken. However, the second resonance, in the case of no proof mass, appears at 7000 Hz that is close to the typical value. The stiffness that was obtained from the experiment

might not realistic. However, the electrical properties are not affected by the broken actuator because the linear model matches well with the experimental data and the capacitance obtained from the experiment is in the range of typical values.

**Table 2** The mechanical and electrical properties of each actuator obtained from the experiment.

Property	Experimental result		
	Electromagnetic LDS V201	Magnetostrictive Extrema AA-050H	Piezoelectric PI P840.60
1. Actuator constant	5.41 N/A	- 109 N/A	0.383 N/V
2. First resonance frequency	93.7 Hz	7541 Hz	1880 Hz
3. Damping ratio (Loss factor)	0.18	(0.091)	0.07
4. Axial stiffness	7340 N/m	32.3 N/ $\mu$ m	1.22 N/ $\mu$ m
5. Moving mass	21.2 g	14.4 g	8.7 g
6. Resistance	3.7 $\Omega$	5.2 $\Omega$	1.5 $\Omega$
7. Inductance	0.4 mH	2.1 mH	-
8. Capacitance	-	-	7 $\mu$ F

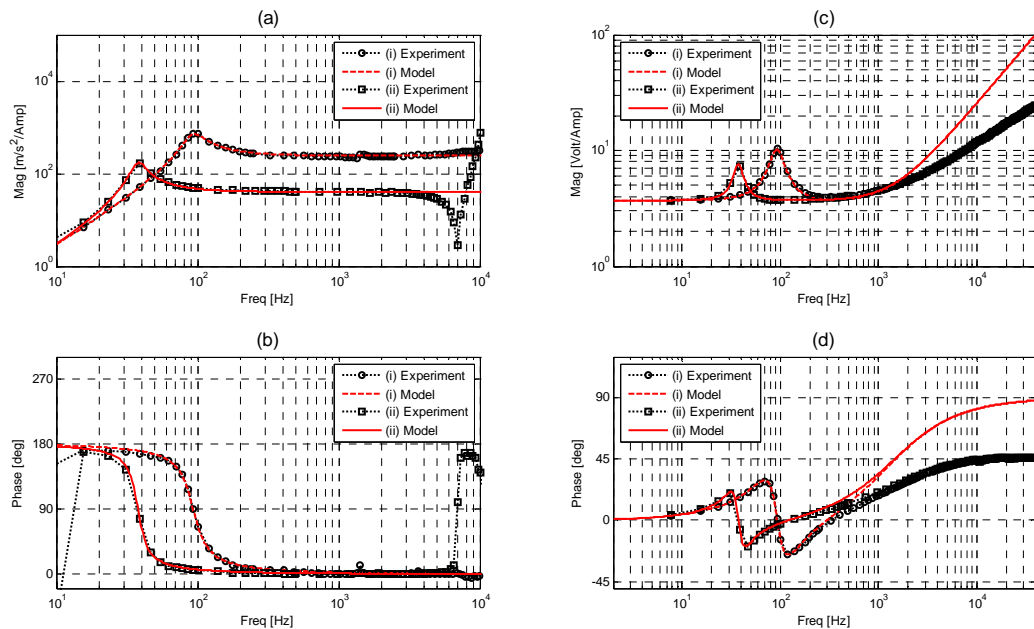


**Figure 18** Experimental result of electromagnetic actuator (i) without and (ii) with proof mass, (a)–(b) The magnitude and phase of acceleration per unit input current and (c)–(d) the magnitude and phase of voltage across the actuator per unit current

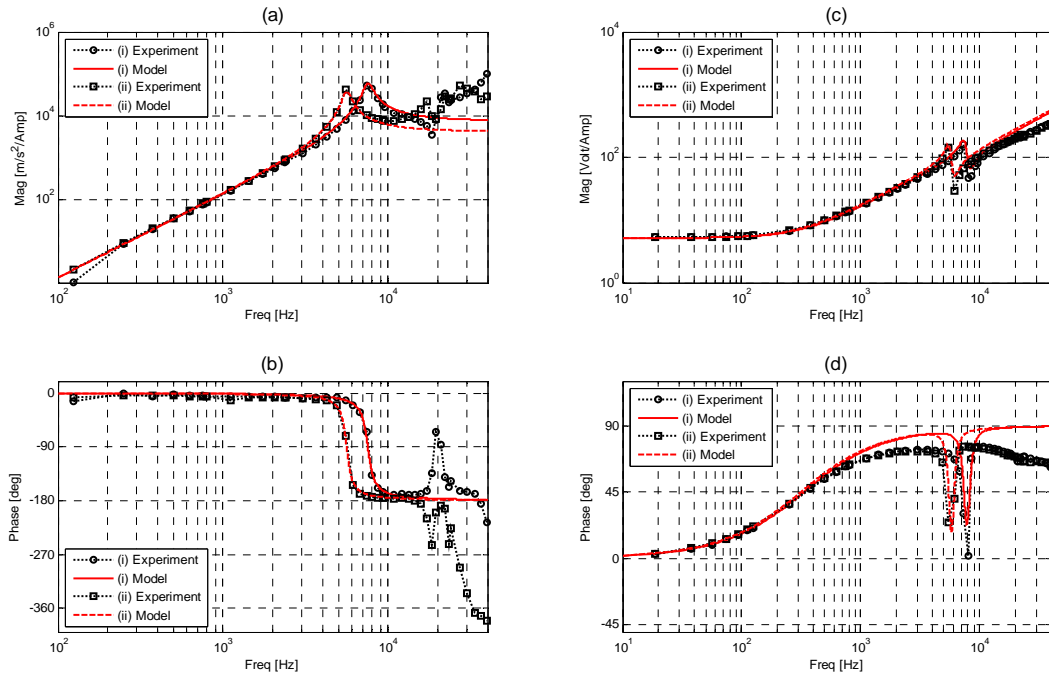


**Figure 19** Experimental result of magnetostrictive actuator (i) without and (ii) with proof mass, (a)–(b) The magnitude and phase of acceleration per unit input current and (c)–(d) the magnitude and phase of voltage across the actuator per unit input current

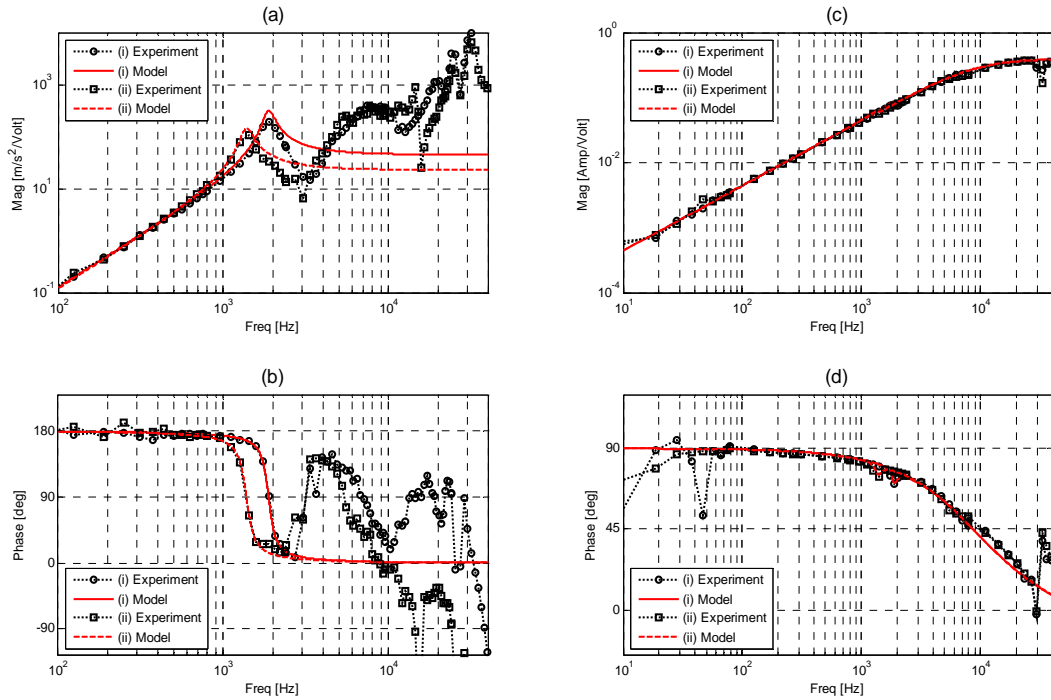


**Figure 20** Experimental result of piezoelectric stack actuator, (a)– (b) The magnitude and phase of acceleration per unit input voltage and (c)–(d) the magnitude and phase of current per unit input voltage

#### 4. Comparison of the actuators

In the previous section, all the actuator parameters have been identified. A further consideration in this section is to compare the mechanical and electrical properties of each actuator. In general, the actuators are compared in terms of the modulus square value of the blocked force per unit electrical power input, the modulus square value of the free displacement per unit electrical power input, and maximum efficiency [1].

Consider the constitutive equation of electromagnetic actuator and magnetostrictive actuator of the form

$$\begin{Bmatrix} F \\ V \end{Bmatrix} = \begin{bmatrix} Z_m & -T \\ T & Z_e \end{bmatrix} \begin{Bmatrix} U \\ I \end{Bmatrix} \quad (33)$$

Assuming the actuator is driven by maximum allowable current  $I_{\max}$ ,  $Z_m = \frac{k}{j\omega}$ , and  $U = j\omega X$  where  $X$  is the displacement, the force-displacement relation can be written as

$$F_D = -F = TI_{\max} - kX. \quad (34)$$

The straight line graph is obtained if the force-displacement relationship is plotted on a linear scale. The force-displacement graph is very important because it indicates the possible operation point.

If the actuator is driven without external load, i.e.,  $F = 0$ , the current is related to the free relative displacement  $X_f$  by:

$$I = \frac{j\omega Z_m X_f}{T}. \quad (35)$$

Substituting this into Eq. (33b) gives the relationship between the electrical voltage and the free displacement:

$$V = j\omega \left( T + \frac{Z_e Z_m}{T} \right) X_f. \quad (36)$$

The electrical power  $P_e$  supplied to the actuator is given by:

$$P_e = \frac{1}{2} \text{Re}\{V I^*\} \quad (37)$$

where  $\text{Re}\{\}$  denotes the real part of a complex number and  $\{\}^*$  denotes the complex conjugate. Substituting (35) and (36) into (37) and rearranging, gives

$$\frac{|X_f|^2}{P_e} = \frac{\frac{2}{\omega^2} |T|^2}{\text{Re}\left\{Z_e + \frac{T^2}{Z_m}\right\}} = \frac{\frac{2}{\omega^4} \left|\frac{A_d}{l}\right|^2}{\text{Re}\left\{\frac{V}{I}\right\}}. \quad (38)$$

Similarly, the modulus squared value of the blocked force per unit input electrical power can be derived using Eq. (33). Setting the relative velocity to zero, the current and voltage are related to the block force  $F_b$  by

$$I = \frac{F_b}{T} \quad (39)$$

and

$$V = Z_e \frac{F_b}{T}. \quad (40)$$

Substituting for Eqs. (39) and (40) into Eq. (37) and rearranging results in

$$\frac{|F_b|^2}{P_e} = \frac{2T^2}{\text{Re}\{Z_e\}}. \quad (41)$$

Consider the mechanical power transmission between the actuator and external load that has the impedance  $Z_L$  as shown in figure 21. The velocity  $U$  can be obtained by Kirchhoff's laws as follows.

$$U = \frac{TI}{Z_m + Z_L} \quad (42)$$

The force transmitted to the load is

$$F_L = Z_L U = \frac{TIZ_L}{Z_m + Z_L} \quad (43)$$

The mechanical power  $P_m$  supplied to the load is given by:

$$P_m = \frac{1}{2} \text{Re}\{F_L U^*\} \quad (44)$$

Substituting Eqs. (42) and (43) into Eq. (44) gives

$$P_m = \frac{\frac{1}{2} T^2 |I|^2}{|Z_m + Z_L|^2} \text{Re}\{Z_L\}. \quad (45)$$

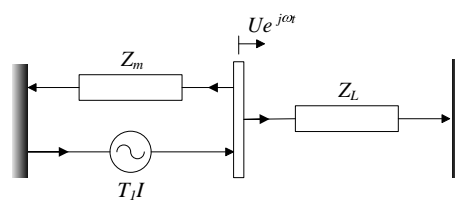


**Figure 21.** Mobility diagram for consideration of power transmission

Letting  $Z_m = R_m + jX_m$  and  $Z_L = R_L + jX_L$  results in

$$P_m = \frac{T^2 |I|^2}{\frac{1}{R_L} (R_m + R_L)^2 + \frac{1}{R_L} (X_m + X_L)^2} \quad (46)$$

Since  $R_m$  and  $R_L$  must be positive but  $X_m$  and  $X_L$  can take any value, the maximum condition of  $P_m$  is  $X_L = -X_m$  and  $\frac{G = (R_m + R_L)^2}{R_L}$  is minimum. Because

$$\frac{dG}{dR_L} = \frac{d}{dR_L} \left( \frac{R_m^2}{R_L} + 2R_m + R_L \right) = -\frac{R_m^2}{R_L^2} + 1,$$

the minimum condition for  $G$  is  $\frac{dG}{dR_L}$  is zero that is  $R_L = R_m$ . Therefore, it can be concluded that the condition for maximum power transmission is  $Z_L = Z_m^*$ . This result is called the matched load [1]. If this condition holds for each actuator then the efficiency can be calculated at this condition; it is defined as the ratio of maximum output of mechanical power to the input electrical power [1]. Substituting  $Z_L = Z_m^*$  in (45) and (42) gives

$$P_m = \frac{T^2 |I|^2}{8 \operatorname{Re}\{Z_m\}} \quad (47)$$

and

$$H = \frac{TI}{2 \operatorname{Re}\{Z_m\}} \quad (48)$$

The velocity of the actuator under matched load conditions is Eq. (48). Substituting Eq. (48) into Eq. (33b), the voltage across the actuator at matched load condition is obtained and is given by

$$V = \left( Z_s + \frac{T^2}{2 \operatorname{Re}\{Z_m\}} \right) I. \quad (49)$$

Furthermore, the input electrical power under this condition is obtained and is given by

$$P_e = \frac{|I|^2}{2} \operatorname{Re} \left\{ Z_e + \frac{T^2}{2 \operatorname{Re}\{Z_m\}} \right\}. \quad (50)$$

The efficiency can be determined by dividing equation Eq. (47) by Eq. (50) and rearranging, to give

$$E = \frac{1}{2 \left( 1 + \frac{2}{T^2} \operatorname{Re}\{Z_m\} \operatorname{Re}\{Z_e\} \right)} \quad (51)$$

For the piezoelectric actuator, the constitutive equation is represented by

$$\begin{Bmatrix} F \\ I \end{Bmatrix} = \begin{bmatrix} Z_m & -T' \\ T' & Z_e^{-1} \end{bmatrix} \begin{Bmatrix} U \\ V \end{Bmatrix}. \quad (52)$$

Following the procedure used for the electromagnetic and magnetostrictive actuators, the following is obtained:

$$F_B = -F = TV_{max} - kX. \quad (53)$$

$$\frac{|X_f|^2}{R_b} = \frac{\frac{2}{\omega^2} \frac{|T'|^2}{|Z_m|}}{\operatorname{Re} \left\{ Z_e^{-1} + \frac{(|T'|)^2}{Z_m} \right\}} = \frac{\frac{2}{\omega^4} \frac{|A_d|^2}{V}}{\operatorname{Re} \left\{ \frac{I}{V} \right\}}. \quad (54)$$

$$\frac{|F_b|^2}{P_e} = \frac{2T^2}{\operatorname{Re}\{Z_e^{-1}\}}. \quad (55)$$

$$E = \frac{1}{2 \left( 1 + \frac{2}{(T')^2} \operatorname{Re}\{Z_m\} \operatorname{Re}\{Z_e^{-1}\} \right)} \quad (56)$$

Now the mechanical and electrical properties of the actuator have been derived and so a comparison can be conducted. The important parameter and equation for each actuator are listed in table 3. The stiffness of piezoelectric actuator in this table is its typical value rather than the experimental result.

**Table 3** The important parameters and equations for each actuator

	Electromagnetic	Magnetostrictive	Piezoelectric
1. Actuator constant	5.41 N/A	- 109 N/A	0.383 N/V
2. Damping ratio (Loss factor)	$\zeta = 0.18$	$(\eta = 0.13)$	$\zeta = 0.07$
3. Axial stiffness	7340 N/m	32.3 N/ $\mu\text{m}$	10 N/ $\mu\text{m}$
4. Moving mass	21.2 g	14.4 g	8.7 g
5. Resistance ( $R$ )	3.7 $\Omega$	5.2 $\Omega$	1.5 $\Omega$
6. Inductance ( $L$ )	0.4 mH	2.1 mH	-
7. Capacitance ( $C$ )	-	-	7 $\mu\text{F}$
8. Max. driven I, V	$I_{\max} = 5$ A	$I_{\max} = 2$ A	$V_{\max} = 200$ V
9. Mechanical Impedance ( $Z_m$ )	$j\omega m_1 + 2\zeta \sqrt{\frac{k}{m_1} + \frac{k}{j\omega}}$	$j\omega m_1 + 2\zeta \sqrt{\frac{k}{m_1} + \frac{k}{j\omega}}$	$j\omega m_1 + 2\zeta \sqrt{\frac{k}{m_1} + \frac{k}{j\omega}}$
10. Electrical Impedance ( $Z_e$ )	$R + j\omega L$	$R + j\omega L$	$R + \frac{1}{j\omega C}$
11. Force-displacement	Equation (34)	Equation (34)	Equation (53)
12. $\frac{ K_f ^2}{P_e}$	Equation (38)	Equation (38)	Equation (54)
13. $\frac{ F_0 ^2}{P_e}$	Equation (41)	Equation (41)	Equation (55)
14. Efficiency	Equation (51)	Equation (51)	Equation (56)

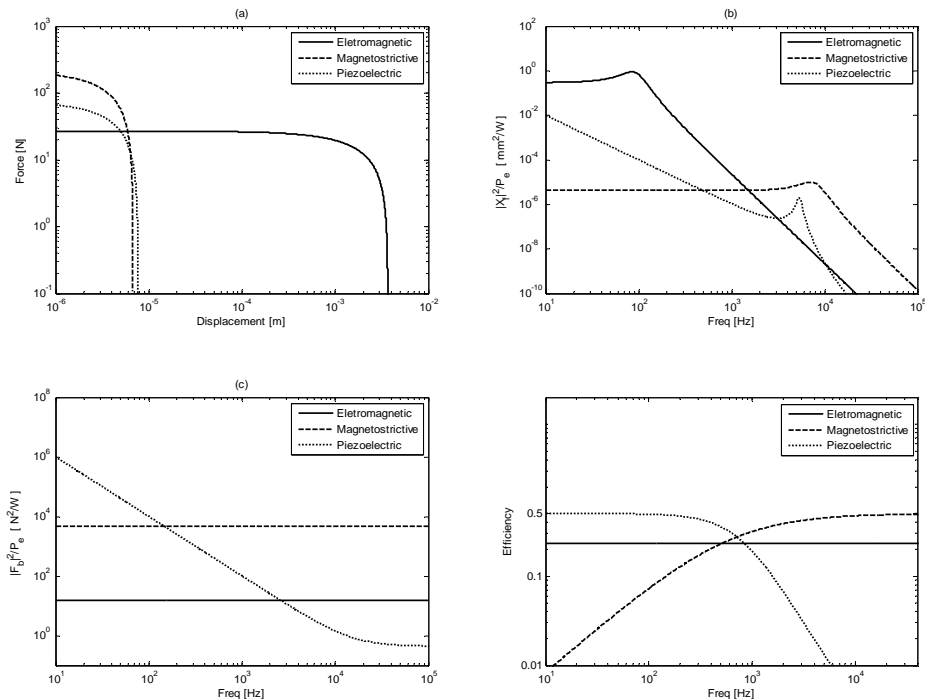


**Figure 22.** (a) Force against displacement, (b) Square of modulus of free displacement per unit input electrical power, (c) square of the modulus of the blocked force per unit input electrical power, (d) Maximum efficiency of the actuators

Figure 22(a) show the force as a function of the displacement calculated using Eq. (34) on logarithmic scale. It would be straight line if it was plotted in linear scale but would be difficult to compare the actuators because of the large difference in blocked force and free displacement. This graph indicates the possible operation point. The actuator cannot operate outside the area covered by force and displacement shown. However, if a gearing mechanism is employed, the force-displacement characteristic can be changed and it may be possible to operate at a point inside the area under the new characteristic graph. The results show that the electromagnetic actuator is suitable for the system that requires a large displacement but low force. Conversely, the magnetostrictive actuator and piezoelectric stack actuator are suitable for the system that requires the large force but small displacement.

Figure 22(b) shows the square of modulus of free displacement per unit input electrical power. The results show that when the actuators operate below their resonance frequencies, the square of the modulus of the free displacement per unit power is constant except for the piezoelectric actuator where it decreases with frequency. The comparison shows that the electromagnetic actuator can generate the largest displacement with the same power consumption for each actuator.

Figure 22(c) show the square of the modulus of the blocked force per unit input electrical power. The results show that the piezoelectric stack actuator is most efficient at low frequency but reduces with frequency. The square of the modulus of the blocked force per unit input electrical power of the electromagnetic actuator and magnetostrictive actuator are constant with frequency but the magnetostrictive actuator is more efficient than the electromagnetic actuator. These results suggest that for the system in which the power supply is limited, the piezoelectric stack actuator is suitable for the system that operates in the low frequency range. The electromagnetic and magnetostrictive actuators are suitable for the system that operates over a large frequency range.

The maximum efficiency graphs are shown in figure 22(d). It can be seen that the maximum efficiency of the electromagnetic actuator is roughly constant with frequency. The maximum efficiency of the magnetostrictive actuator increases with frequency. Conversely, the maximum efficiency of the piezoelectric stack actuator decreases with frequency. In both cases the maximum efficiency is 0.5 that is the maximum possible value predicted by maximum power transfer theorem [8]. It should be noted that below the resonance frequency of an actuator, the mechanical impedance is simply a stiffness and so a matched load should be a mass that depends on the operational frequency. Therefore, this analysis is applicable in a practical sense if the primary disturbance is at a single frequency.

In this section, the mechanical and electrical properties of the actuators have been compared. The criteria in this section might be used as a guideline for selecting an actuator in the system design process. It should be noted that there might be other criteria that could be used to compare the actuator depending on the constraints of the application.

## **5. Application in active vibration isolation system**

In this section, the application of actuators in an active vibration isolation system is demonstrated. A sky-hook-damper that is known as a simple, robust and effective controller is used in the demonstration. The system is assumed to be a single-axis active vibration isolation system. The robust stability criteria is employed to test the stability of the system because the identification showed that the linear model of the actuators cannot predict the experimental results very well. The identification error is treated as unstructured uncertainty. Since the actuator is also driven with a current or a voltage driver, the effect of these two different types of driver is investigated.

### **5.1 Stability consideration**

Consider a linear time invariant system  $G(s)$  subject to unstructured uncertainty  $\Delta(s)$  as shown in figure 23 where  $u$  is the control input to the actuator that might be

current or voltage,  $w$  is the disturbance input from ground that is defined by the ground velocity,  $z$  is the performance output that is the payload velocity,  $y$  is the measurement output that is the acceleration of the payload,  $q$  is the uncertainty input and  $p$  is the uncertainty output. It is assumed that  $\Delta(s)$  is an unknown transfer function that is stable and  $\|\Delta(j\omega)\| \leq 1$ .

The objective of this section is to design a controller  $K(s)$  that minimizes the transmissibility. In this case, the equivalent sky-hook-damper control is an integral acceleration feedback control. The control law is given by

$$u = -K(s)y = g \frac{1}{s+a} y \quad (57)$$

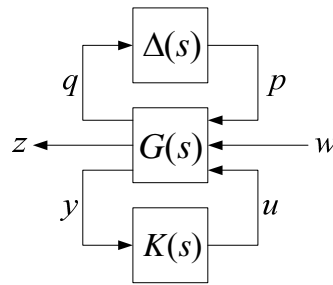


**Figure 23** Element of the robust control problem

If the plant  $G(s)$  is partitioned by

$$G(s) = \begin{bmatrix} G_{qp}(s) & G_{qw}(s) & G_{qy}(s) \\ G_{zp}(s) & G_{zw}(s) & G_{zy}(s) \\ G_{yp}(s) & G_{yw}(s) & G_{yu}(s) \end{bmatrix}. \quad (58)$$

the close loop system can be written by

$$\begin{bmatrix} q \\ z \end{bmatrix} = \frac{1}{1 + K(s)G_{yu}(s)} \begin{bmatrix} H_{qp}(s) & H_{qw}(s) \\ H_{zp}(s) & H_{zw}(s) \end{bmatrix} \begin{bmatrix} p \\ w \end{bmatrix} \quad (59a)$$

or equivalently

$$\begin{bmatrix} Q \\ Z \end{bmatrix} = \begin{bmatrix} T_{QP}(s) & T_{QW}(s) \\ T_{ZP}(s) & T_{ZW}(s) \end{bmatrix} \begin{bmatrix} P \\ W \end{bmatrix} \quad (59b)$$

where

$$T_{QP}(s) = \frac{H_{QP}(s)}{1 + K(s)G_{YU}(s)},$$

$$T_{QW}(s) = \frac{H_{QW}(s)}{1 + K(s)G_{YU}(s)},$$

$$T_{ZP}(s) = \frac{H_{ZP}(s)}{1 + K(s)G_{YU}(s)},$$

$$T_{ZW}(s) = \frac{H_{ZW}(s)}{1 + K(s)G_{YU}(s)},$$

$$H_{QP}(s) = G_{QP}(s) + G_{QP}(s)K(s)G_{YU}(s) + G_{QY}(s)K(s)G_{YP}(s),$$

$$H_{ZP}(s) = G_{ZP}(s) + G_{ZP}(s)K(s)G_{YU}(s) + G_{ZY}(s)K(s)G_{YP}(s),$$

$$H_{QW}(s) = G_{QW}(s) + G_{QW}(s)K(s)G_{YU}(s) + G_{QY}(s)K(s)G_{YW}(s) \text{ and}$$

$$H_{ZW}(s) = G_{ZW}(s) + G_{ZW}(s)K(s)G_{YU}(s) + G_{ZY}(s)K(s)G_{YW}(s).$$

*Nominal stability*

Let  $\lambda_i$  be the poles of the characteristic equation  $1 + K(s)G_{YU}(s)$ , the system given by Eq. (59a) is stable if and only if

$$\text{Re}\{\lambda_i\} \leq 0. \quad (60)$$

In this study, the control law is given in Eq. (57) and the characteristic equation becomes

$$1 + g \left( \frac{1}{s + \alpha} G_{YU}(s) \right) \quad (61)$$

that root locus can be used to determine the maximum allowable controller gain  $g$  of the nominal system when the scalar  $\alpha$  is specified.

*Robust stability*

The system described by Eqs. (59a) and (59b) is robust stable if  $T_{QP}$  is stable and there exists some scaling matrix  $S \in R^{n \times n}$  such that [9]

$$\left\| S^{\frac{1}{2}} T_{qp}(j\omega) S^{-\frac{1}{2}} \right\| \leq 1 \quad (62a)$$

for all circular frequency  $\omega$ . Let  $T_{qp} = D_{qp} + C_q(sI^{n \times n} - A)^{-1} B_p$  where  $A \in R^{n \times n}$ ,  $D_{qp} \in R^{n_1 \times n_1}$ ,  $n_1$  is number of input and output of uncertainty channels, the condition in Eq.(62a) is equivalent to the existence of matrices  $P = P^T > 0$  and  $S = \text{diag}(s_1, s_2, \dots, s_{n_1}) > 0$  that satisfy [9]

$$\begin{bmatrix} A^T P + P A & P B_p & C_q^T S \\ B_p^T P & S & D_{qp}^T S \\ S C_q & S D_{qp} & -S \end{bmatrix} < 0 \quad (62b)$$

The linear matrix inequality in Eq. (62b) is convex in  $P$  and  $S$  and can be solved by available software, e.g., LMI lab of MATLAB.

#### Nominal performance

The nominal transmissibility  $\Gamma_N(\omega)$  of the system without the uncertainty at each frequency  $\omega$  can be obtained by

$$\Gamma_N(\omega) = \|T_{zw}(j\omega)\|. \quad (62)$$

#### Robust performance

Let

$$\begin{aligned} \begin{bmatrix} q(s) \\ z(s) \end{bmatrix} &= \begin{bmatrix} T_{qp}(s) & T_{qw}(s) \\ T_{zp}(s) & T_{zw}(s) \end{bmatrix} \begin{bmatrix} p(s) \\ w(s) \end{bmatrix} \\ &= \left( \begin{bmatrix} D_{qp} & D_{qw} \\ D_{zp} & D_{zw} \end{bmatrix} + \begin{bmatrix} C_q \\ C_z \end{bmatrix} (sI^{n \times n} - A)^{-1} \begin{bmatrix} B_p & B_w \end{bmatrix} \right) \begin{bmatrix} p(s) \\ w(s) \end{bmatrix} \end{aligned} \quad (63a,b)$$

$$p(s) = \Delta(s)q(s), \quad \|\Delta(j\omega)\|_{\infty} \leq 1,$$

the system described by Eq. (63a,b) is quadratically stable and  $\|T_{zw}(j\omega)\|_{\infty} \leq \gamma$  if there exist matrices  $P = P^T > 0$  and  $S = \text{diag}(s_1, s_2, \dots, s_{n_1}) > 0$  that satisfy

$$\begin{bmatrix} A^T P + PA & PB_p & PB_w & C_q^T S & C_z^T \\ B_p^T P & -S & 0 & D_{qp}^T S & D_{zp}^T \\ B_w^T P & 0 & -\gamma I & D_{qw}^T S & D_{zw}^T \\ SC_q & SD_{qp} & SD_{qw} & -S & 0 \\ C_z & D_{zp} & D_{zw} & 0 & -\gamma I \end{bmatrix} \prec 0. \quad (64)$$

If  $P$  and  $S$  satisfy (64) and also minimize  $\gamma$ , the robust transmissibility  $\Gamma(\omega)$  can be obtained by

$$\Gamma(\omega) = \bar{\sigma} \left( \begin{bmatrix} S & 0 \\ 0 & 1 \end{bmatrix}^{\frac{1}{2}} \begin{bmatrix} T_{qp}(j\omega) & T_{qw}(j\omega) \\ T_{zp}(j\omega) & T_{zw}(j\omega) \end{bmatrix} \begin{bmatrix} S & 0 \\ 0 & 1 \end{bmatrix}^{-\frac{1}{2}} \right) \quad (65)$$

where  $\bar{\sigma}(\cdot)$  denote the maximum singular value.

## 5.2 Active control demonstration

Referring to the constitutive Eqs (5) and (12), it is supposed that the constitutive equations including unstructured uncertainty in the Laplace domain can be written as

$$F(s) = \frac{1}{s} Z_m(s) A(s) - (1 + W_m(s) \Delta_m(s)) T I(s) \quad (66a)$$

$$V(s) = \frac{1}{s} T A(s) + \frac{1}{(1 + W_s(s) \Delta_s(s))} Z_s I(s) \quad (66b)$$

where  $\Delta_m(s)$  and  $\Delta_s(s)$  are the normalized unstructured uncertainty which  $\|\Delta_m\| \leq 1$  and  $\|\Delta_s\| \leq 1$  and  $W_m(s)$  and  $W_s(s)$  are weighting transfer functions. If the actuator is driven without an external load, i.e.,  $F(s) = 0$ , the current  $I(s)$  is related to the free relative acceleration  $A(s)$  by:

$$\frac{A(s)}{I(s)} = (1 + W_m(s) \Delta_m(s)) \frac{sT}{Z_m(s)} \quad (67a)$$

or

$$W_m(s) \Delta_m(s) = \frac{\left( \frac{A(s)}{I(s)} \right)}{\left( \frac{sT}{Z_m(s)} \right)} - 1. \quad (67b)$$

$\frac{A(s)}{I(s)}$  is obtained by the experimental result and  $\frac{sT}{Z_m(s)}$  is the linear approximation model that has been identified. Dividing Eq. (66b) by  $I(s)$  and rearranging, gives

$$W_e(s)\Delta_e(s) = \frac{Z_e}{\frac{V(s)}{I(s)} - \frac{TA(s)}{sI(s)}} - 1 \quad (68)$$

where  $\frac{V(s)}{I(s)}$  and  $\frac{A(s)}{I(s)}$  are the experimental results and  $Z_e$  and  $T$  are known. Figure 24 show the uncertainties  $W_m\Delta_m$  and  $W_e\Delta_e$  obtained by the experimental results and the weighting transfer functions  $W_m$  and  $W_e$  of the electromagnetic actuator and magnetostrictive actuators. The weighting transfer functions of electromagnetic actuator are given by

$$W_m(s) = \frac{3.41 \times 10^{-2}s + 0.15}{1.59 \times 10^{-2}s + 1} \quad (69a)$$

$$W_e(s) = \frac{17.51 \times 10^{-2}s + 0.022}{7.96 \times 10^{-2}s + 1} \quad (69b)$$

and the weighting transfer functions of magnetostrictive actuator are given by

$$W_m(s) = \frac{4.38 \times 10^{-2}s + 0.055}{1.99 \times 10^{-6}s + 1} \quad (70a)$$

$$W_e(s) = \frac{2.23 \times 10^{-2}s + 0.028}{1.59 \times 10^{-2}s + 1} \quad (70b)$$

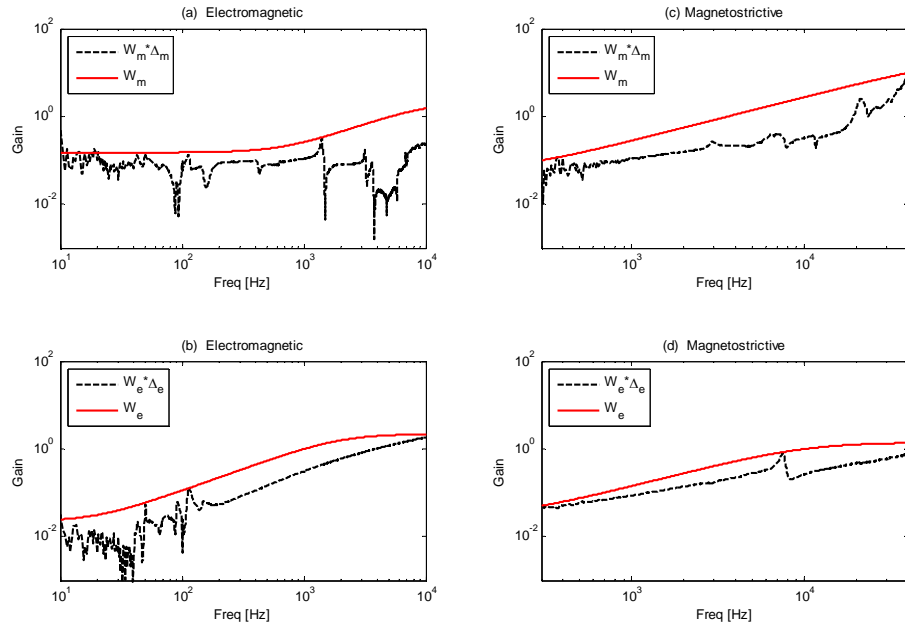


**Figure 24.** Uncertainty and weighting transfer function of the electromagnetic and magnetostrictive actuators.



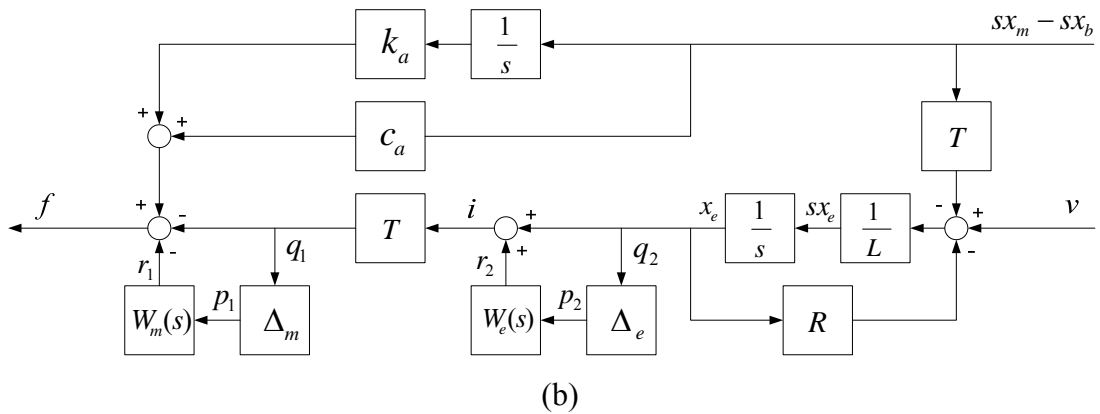


**Figure 26** Block diagram of the actuator when it is driven by (a) current driven or (b) voltage driver

Referring to equation (66), an alternative form can be represented by

$$f(s) = (c_a a + k_a a/s) [s x_m(s) - s x_b(s)] - (1 + W_m(s) \Delta_m(s)) T I(s) \quad (7)$$

1a  
)

(7

1b

)

where  $k_a$  and  $c_a$  are the actuator stiffness and actuator damping coefficient respectively.  $s x_m - s x_b$  is the relative velocity of point  $m$  respect to point  $b$ . If the actuator is driven by the current driver, the equivalent block diagram is shown in figure 26a. On the other hand, if it is driven by the voltage driver, the equivalent block diagram is shown in figure 26b.

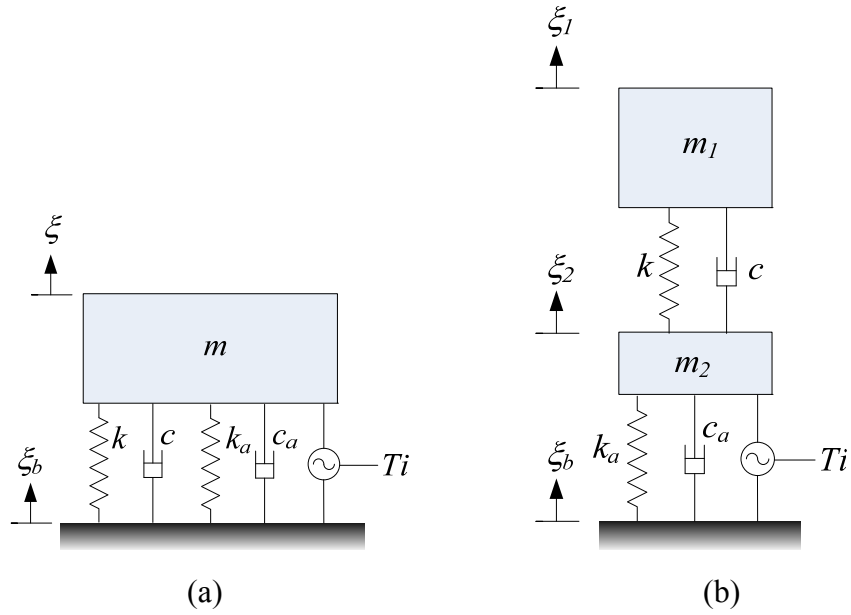


**Figure 27** Single axis active vibration isolation system using (a) soft-actuator and (b) stiff-actuator

In single axis active vibration isolation system, the application of the soft-actuator and stiff-actuator are shown in figure 27a and 27b respectively [10]. At first, the application of the soft actuator in the active vibration isolation system is considered. Consider figure 27a, the equation of motion of mass  $m$  in the Laplace domain is given by

$$s^2 \xi = -\frac{c}{m}(s\xi - s\xi_b) - \frac{k}{m}(\xi - \xi_b) - \frac{1}{m}f \quad (72)$$

where  $f$  is an actuator force. In figure 26a and 26b,  $x_m = \xi$ ,  $x_b = \xi_b$  and the actuator force is given by

$$f = c_a(s\xi - s\xi_b) - k_a(\xi - \xi_b) - r_1 - TL \quad (73)$$

Letting  $x_1 = s\xi$ ,  $x_2 = \xi - \xi_b$  and  $w = s\xi$  the state-space model of the system in figure 27a, which the actuator is driven by the current driver can be written as

$$s \begin{pmatrix} x_1 \\ x_2 \end{pmatrix} = \begin{bmatrix} -\frac{c+c_a}{m} & -\frac{k+k_a}{m} \\ 1 & 0 \end{bmatrix} \begin{pmatrix} x_1 \\ x_2 \end{pmatrix} + \begin{bmatrix} \frac{1}{m} & \frac{c+c_a}{m} & \frac{T}{m} \\ 0 & -1 & 0 \end{bmatrix} \begin{pmatrix} W_m(s)p \\ w \\ t \end{pmatrix} \quad (74)$$

$$\begin{Bmatrix} q_1 \\ z \\ y \end{Bmatrix} = \begin{bmatrix} 0 & 0 \\ 1 & 0 \\ -\frac{c + c_a}{m} & -\frac{k + k_a}{m} \end{bmatrix} \begin{Bmatrix} x_1 \\ x_2 \end{Bmatrix} + \begin{bmatrix} 0 & 0 & 0 \\ 0 & 0 & 0 \\ \frac{1}{m} & \frac{c + c_a}{m} & \frac{T}{m} \end{bmatrix} \begin{Bmatrix} W_m(s)p_1 \\ W \\ l \end{Bmatrix}$$

$$p_1 = \Delta_m(s)q_1.$$

From figure 26b, the current is related to the input voltage  $v$  and relative velocity  $s\xi - s\xi_b$  by

$$s x_e = -\frac{R}{L}x_e - \frac{T}{L}(s\xi - s\xi_b) + \frac{1}{L}v \quad (75a)$$

$$l = x_e + r_2. \quad (75b)$$

Letting  $x_1 = s\xi$ ,  $x_2 = \xi - \xi_b$  and  $w = s\xi_b$ , Eqs. (72), (73), (75) and figure 26b give

$$s \begin{Bmatrix} x_1 \\ x_2 \\ x_e \end{Bmatrix} = \begin{bmatrix} -\frac{c + c_a}{m} & -\frac{k + k_a}{m} & \frac{T}{m} \\ 1 & 0 & 0 \\ \frac{1}{m} & \frac{c + c_a}{m} & \frac{T}{m} \end{bmatrix} \begin{Bmatrix} x_1 \\ x_2 \\ x_e \end{Bmatrix} + \begin{bmatrix} \frac{1}{m} & \frac{T}{m} & \frac{c + c_a}{m} & 0 \\ 0 & 0 & 1 & 0 \\ 0 & 0 & \frac{T}{L} & \frac{1}{L} \end{bmatrix} \begin{Bmatrix} W_m(s)p_1 \\ W_a(s)p_2 \\ w \\ v \end{Bmatrix} \quad (76)$$

$$\begin{Bmatrix} q_1 \\ q_2 \\ z \\ y \end{Bmatrix} = \begin{bmatrix} 0 & 0 & T \\ 0 & 1 & 0 \\ -\frac{c + c_a}{m} & -\frac{k + k_a}{m} & \frac{T}{m} \end{bmatrix} \begin{Bmatrix} x_1 \\ x_2 \\ x_e \end{Bmatrix} + \begin{bmatrix} 0 & T & 0 & 0 \\ 0 & 0 & 0 & 0 \\ 1 & \frac{T}{m} & \frac{c + c_a}{m} & 0 \end{bmatrix} \begin{Bmatrix} W_m(s)p_1 \\ W_a(s)p_2 \\ w \\ v \end{Bmatrix}$$

$$\begin{Bmatrix} p_1 \\ p_2 \end{Bmatrix} = \begin{bmatrix} \Delta_m(s) & 0 \\ 0 & \Delta_a(s) \end{bmatrix} \begin{Bmatrix} q_1 \\ q_2 \end{Bmatrix}$$

which is the state-space model of the system in figure 27a, in which the actuator is driven by the voltage driver. Assuming,  $m = 50$  kg,  $c = 40$  N-s/m,  $k = 50\,000$  N/m and from the identification results, it is known that  $k_a = 7340$  N/m,  $c_a = 4.5$  N-s/m,  $T = 5.41$  N/A,  $R = 3.7 \Omega$  and  $L = 0.4$  mH. Substituting into Eqs. (74) and (76) and the system equations are converted to the transfer matrix realization of the form in Eq. (58). To design the controller in Eq. (57), if the measuring signal has low drift and very small offset, the integral constant  $\alpha$  can be considered to be small. In this demonstration it is assumed that  $\alpha = 0.1$ . The desired damping ratio can be achieved by a suitable value of controller gain  $g$  that might be obtained by root locus

plot. Let *system 1* and *system 2* refer to the systems in Eqs. (74) and (76) with integral acceleration feedback respectively. Using Eq. (61), the corresponding root locus of *system 1* and *system 2* are represented in figures 28 and 29 respectively. The root loci show that gain margin of both systems is infinity. However, in practice, the controller gain can only be increased until  $\|T_{sp}\|_{\infty} < 1$  because the systems are subjected to the uncertainty. Actually, the gain margin is finite in robust stability sense.

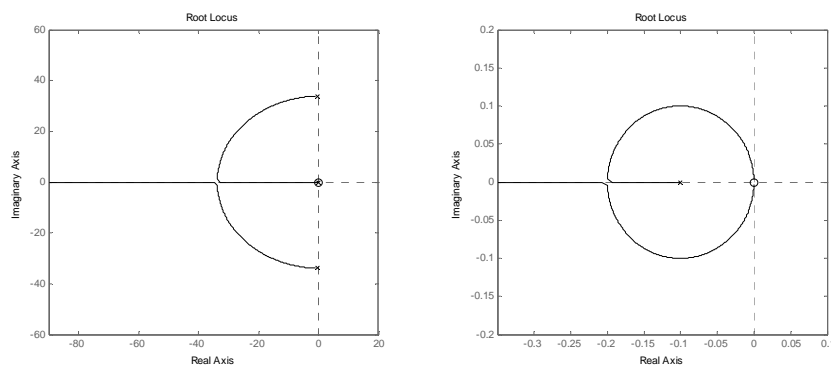


**Figure 28** Root locus of *system 1* (the right hand side picture zooms in the locus near the origin)

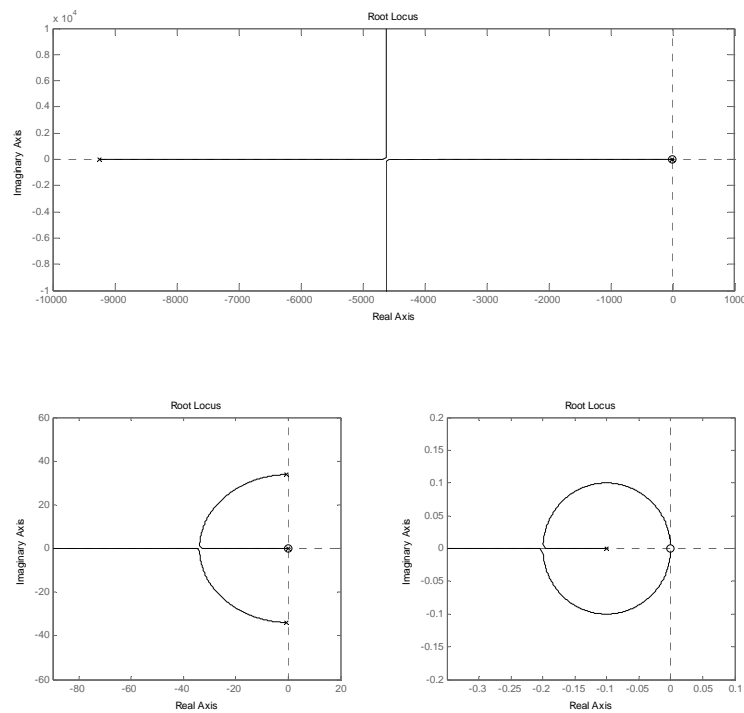


**Figure 29** Root locus of *system 2* (the two lower plots show a zoom near the origin)

When the active vibration isolation system is subject to uncertainty, the best transmissibility that can be achieved is the nominal transmissibility and the worst transmissibility is not worse than the robust transmissibility. Figures 30 and 31 show the robust stability plot of  $(\|S^{-1}T_{qp}(\omega)S^{-1}\|)$  and the nominal and robust transmissibility of *system 1* and *system 2* using different controller gains. The arrows indicate the direction of gain increasing. The system is still stable when the controller gain is increased. A better nominal transmissibility is achieved when the controller gain is increased; however, the robust performance deteriorates when the controller gain is increased. Figure 32 shows a comparison of the robust stability and robust performance of two systems that use different kinds of driver. In this comparison, the controller gains are set to achieve the damping ratio  $\zeta = 1$ . The nominal transmissibilities are similar, but the robust performance of the system that uses the current driver is better than the system that use voltage driver. Clearly, to use the current driver is ideal with only one source of uncertainty. To improve the robust performance of the system that uses a voltage driver, a more sophisticated controller might be used.

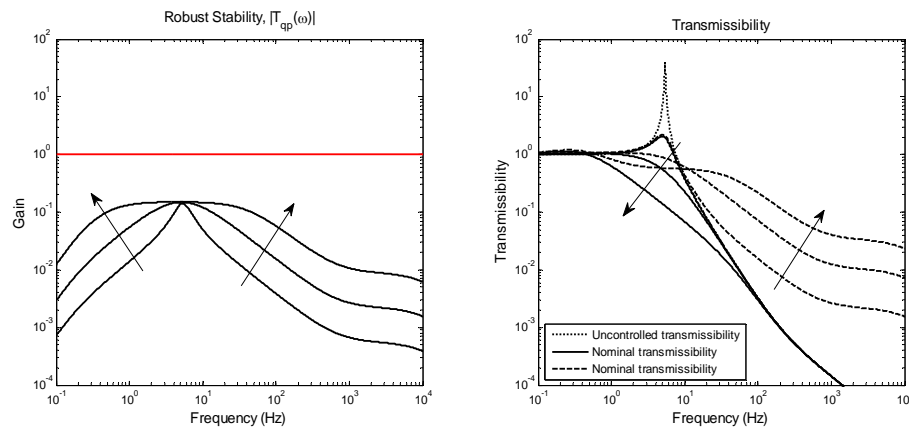


**Figure 30** Robust stability and robust performance plot of *system 1* using gain  $g = 150, 600, 2400$  (arrows indicate the direction of increasing gain)

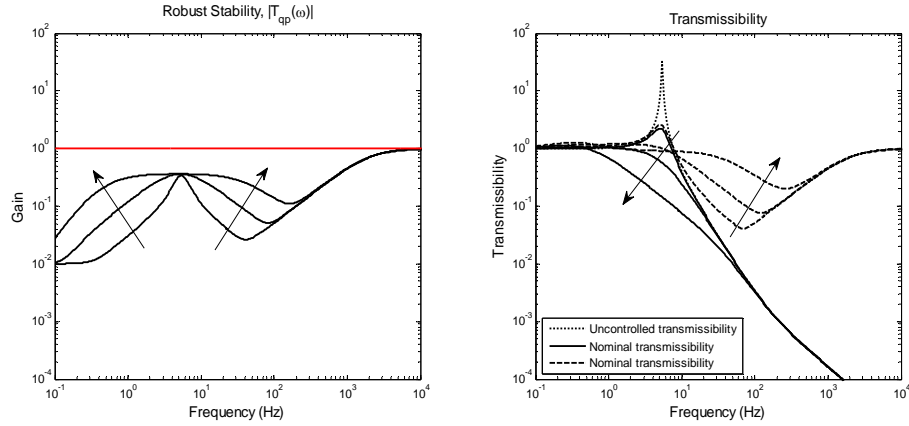


**Figure 31** Robust stability and robust performance plot of *system 2* using gain  $g = 500, 2000, 8000$  (arrows indicate the direction of increasing gain)

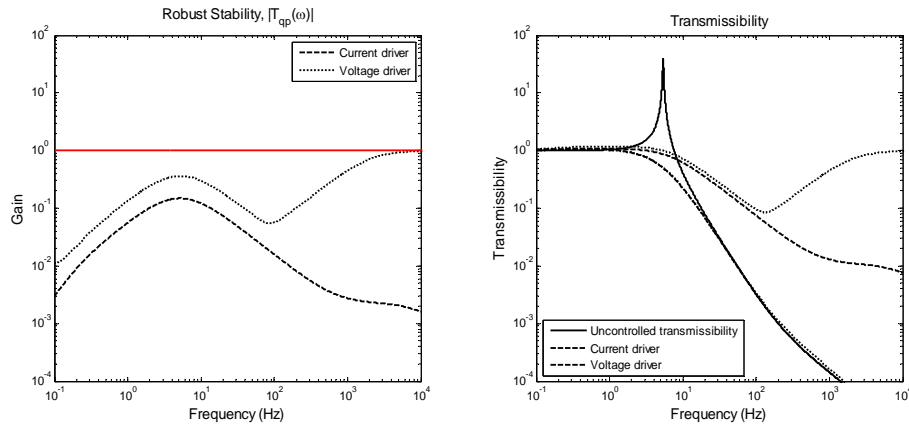


**Figure 32** Robust stability and robust performance plot of the *system 1* and *system 2*

Next, a stiff-actuator is applied in an active vibration isolation system. Consider figure 27b, the equations of motion of mass  $m_1$  and  $m_2$  in the Laplace domain are given by

$$s^2 \xi_1 = -\frac{c}{m_1} (s \xi_1 - s \xi_2) - \frac{k}{m_1} (\xi_1 - \xi_2) \quad (77a)$$

$$s^2 \xi_2 = \frac{c}{m_2} (s \xi_1 - s \xi_2) + \frac{k}{m_2} (\xi_1 - \xi_2) - \frac{1}{m_2} f \quad (77b)$$

where  $f$  is an actuator force. In figure 26a and 26b,  $x_m = \xi_2$ ,  $x_b = \xi_b$  and the actuator force is given by

$$f = c_c (s \xi_2 - s \xi_b) + k_a (\xi_2 - \xi_b) - r_1 - Tl \quad (78)$$

Let  $x_1 = s\xi_1$ ,  $x_2 = \xi_1 - \xi_2$ ,  $x_3 = s\xi_2$ ,  $x_4 = \xi_2 - \xi_b$  and  $W = s\xi_b$ , the state-space model of the system in figure 27b, in which the actuator is driven by the current driver is given by

$$\begin{aligned} \begin{Bmatrix} x_1 \\ x_2 \\ x_3 \\ x_4 \end{Bmatrix} &= \begin{bmatrix} \frac{c}{m_1} & \frac{k}{m_1} & \frac{c}{m_1} & 0 \\ 1 & 0 & -1 & 0 \\ \frac{c}{m_2} & \frac{k}{m_2} & -\frac{c+c_a}{m_2} & -\frac{k_a}{m_2} \\ 0 & 0 & 1 & 0 \end{bmatrix} \begin{Bmatrix} x_1 \\ x_2 \\ x_3 \\ x_4 \end{Bmatrix} + \begin{bmatrix} 0 & 0 & 0 \\ 0 & 0 & 0 \\ \frac{1}{m_2} & \frac{c_a}{m_2} & \frac{T}{m_2} \\ 0 & -1 & 0 \end{bmatrix} \begin{Bmatrix} W_m(s)p_1 \\ W \\ l \end{Bmatrix} \\ \begin{Bmatrix} q_1 \\ z \end{Bmatrix} &= \begin{bmatrix} 0 & 0 & 0 & 0 \\ 1 & 0 & 0 & 0 \\ -\frac{c}{m_1} & -\frac{k}{m_1} & \frac{c}{m_1} & 0 \end{bmatrix} \begin{Bmatrix} x_1 \\ x_2 \\ x_3 \\ x_4 \end{Bmatrix} + \begin{bmatrix} 0 & 0 & T \\ 0 & 0 & 0 \\ 0 & 0 & 0 \end{bmatrix} \begin{Bmatrix} W_m(s)p_1 \\ W \\ l \end{Bmatrix} \\ p_1 &= \Delta_m(s)q_1. \end{aligned} \quad (79)$$

If the actuator of the system in figure 27b is driven by a voltage driver, the state-space model becomes

$$\begin{aligned} sx &= \begin{bmatrix} -\frac{c}{m_1} & -\frac{k}{m_1} & \frac{c}{m_1} & 0 & 0 \\ 1 & 0 & -1 & 0 & 0 \\ \frac{c}{m_2} & \frac{k}{m_2} & -\frac{c+c_a}{m_2} & -\frac{k_a}{m_2} & \frac{T}{m_2} \\ 0 & 0 & 1 & 0 & 0 \\ 0 & 0 & -\frac{T}{L} & 0 & -\frac{R}{L} \end{bmatrix} x + \begin{bmatrix} 0 & 0 & 0 & 0 \\ 0 & 0 & 0 & 0 \\ \frac{1}{m_2} & \frac{T}{m_2} & \frac{c_a}{m_2} & 0 \\ 0 & 0 & -1 & 0 \\ 0 & 0 & \frac{T}{L} & \frac{1}{L} \end{bmatrix} \begin{Bmatrix} r_1 \\ r_2 \\ W \\ v \end{Bmatrix} \\ \begin{Bmatrix} q_1 \\ z \end{Bmatrix} &= \begin{bmatrix} 0 & 0 & 0 & 0 & T \\ 0 & 0 & 0 & 0 & 1 \\ 1 & 0 & 0 & 0 & 0 \\ -\frac{c}{m_1} & -\frac{k}{m_1} & \frac{c}{m_1} & 0 & 0 \end{bmatrix} x + \begin{bmatrix} 0 & T & 0 & 0 \\ 0 & 0 & 0 & 0 \\ 0 & 0 & 0 & 0 \\ 0 & 0 & 0 & 0 \end{bmatrix} \begin{Bmatrix} r_1 \\ r_2 \\ W \\ v \end{Bmatrix} \\ \begin{Bmatrix} r_1 \\ r_2 \end{Bmatrix} &= \begin{bmatrix} W_m(s) & 0 \\ 0 & W_a(s) \end{bmatrix} \begin{Bmatrix} p_1 \\ p_2 \end{Bmatrix}, \quad \begin{Bmatrix} p_1 \\ p_2 \end{Bmatrix} = \begin{bmatrix} \Delta_m(s) & 0 \\ 0 & \Delta_a(s) \end{bmatrix} \begin{Bmatrix} q_1 \\ q_2 \end{Bmatrix} \end{aligned} \quad (80)$$

where  $x^T = [x_1^T \ x_2^T \ x_3^T \ x_4^T \ x_5^T]$

Assuming,  $m_1 = 50$  kg,  $m_2 = 10$  kg,  $c = 40$  N-s/m,  $k = 50\,000$  N/m and from the identification results of magnetostrictive actuator, it is known that  $k_a = 32.3$  N/ $\mu\text{m}$ ,  $c_a = 85$  N-s/m,  $T = -109$  N/A,  $R = 5.2\ \Omega$  and  $L = 2.1$  mH. Substituting into Eqs. (79) and (80) the system is converted to the transfer matrix realization of the form given in Eq. (58). Let *system 3* and *system 4* refer to the system given in Eqs.(79) and (80) with integral acceleration feedback respectively. Because

$T$  is negative the controller gain  $g = -h$ , Using Eq. (61) and letting  $\alpha = 0.1$ , the corresponding root loci of *system 3* and *system 4* are shown in figure 33 and 34 respectively. The open-loop transfer function of each system has two coupled complex poles that imply each system has two resonant frequencies. From the root loci plots in figure 33 and 34, it can be seen that if the controller gains are increased, the damping ratio of the first resonant frequency will be increased but the damping ratio of the second resonance will be decreased and the controlled systems will be unstable if high controller gain is selected. The gain margins of *system 3* and *system 4* are 7340 A/(m/s) and 195,000 V/(m/s) (or  $195000 / 5.4 \text{ (V}/\Omega\text{)}/(\text{m/s}) = 37500 \text{ A}/(\text{m/s})$ ) respectively. If the design objective desires the damping ratio of the first resonant frequency to be equal to 1, *system 4* will be able to achieve this objective but *system 3* is not able to achieve this because the desired controller gain is over the gain margin. The possible maximum damping ratio of the first resonance frequency of *system 3* is 0.21. In equation (71b), the term  $\frac{1}{sL + R}$  acts as a low pass filter such that high frequency input is filtered out and is not allowed to excite the second resonance frequency. As a result, this is the reason why the gain margin of *system 4* is higher than that of *system 3*.

By trial and error, it is known that gain margin can be increased by adding an external damper parallel with the actuator. Assume the external damping  $c_e = 12\,500$  N-s/m is added so the total damping of the actuator is  $c_a = 85 + 12\,500 = 12\,585$  N-s/m. Using Eq. (61) and letting  $\alpha = 0.1$ , the corresponding root loci of *system 3* and *system 4* with an external damper are shown in figures 35 and 36 respectively. It can be seen that the gain margin of *system 3* becomes infinite and the gain margin of *system 4* is increased by a factor of about ten.

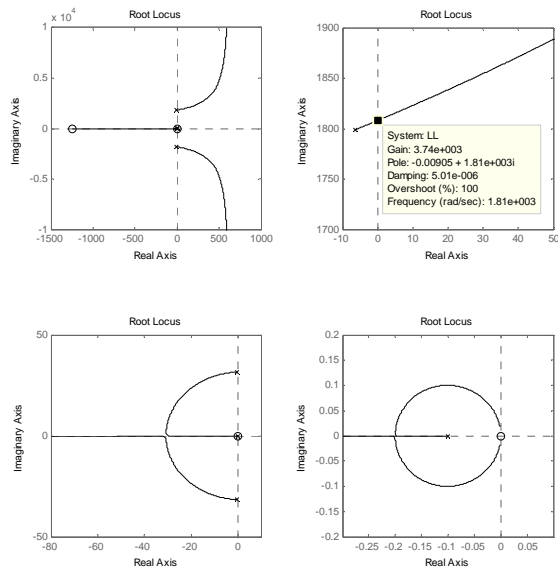


**Figure 33** Root locus of system 3

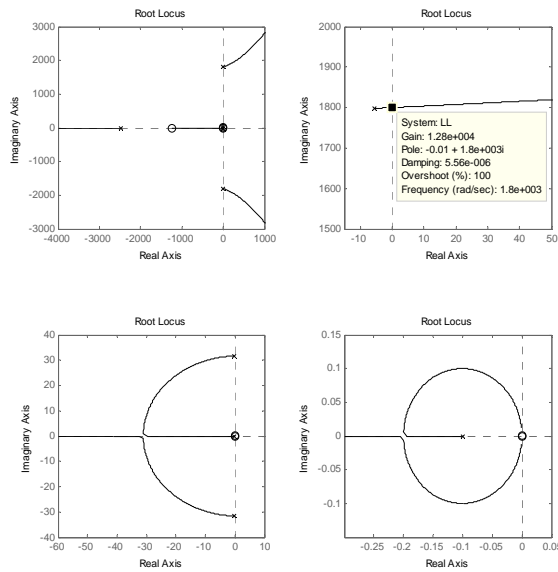


**Figure 34** Root locus of the system 4

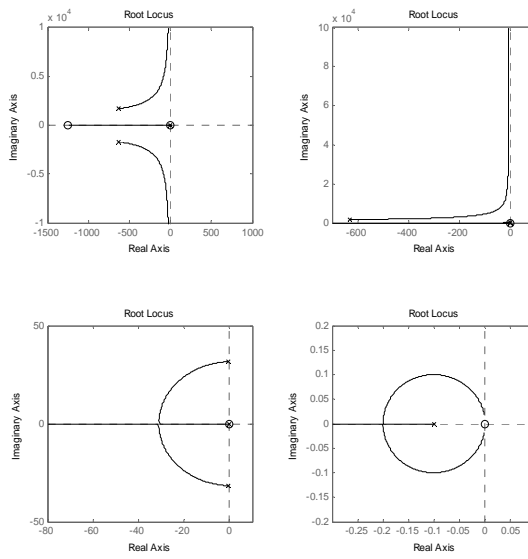


**Figure 35** Root locus of *system 3* with external damper

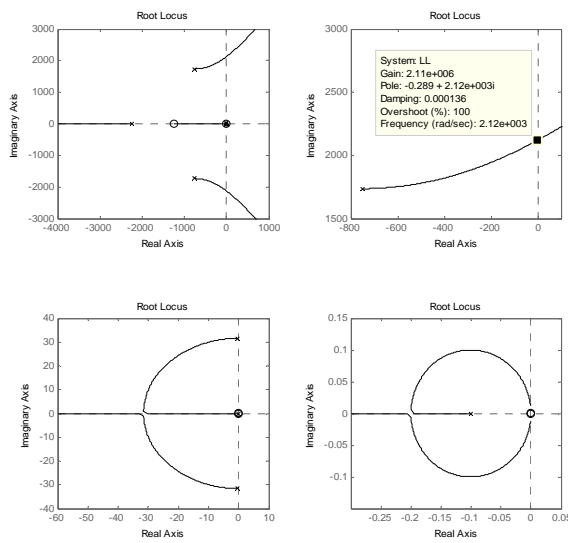


**Figure 36** Root locus of *system 4* with external damper

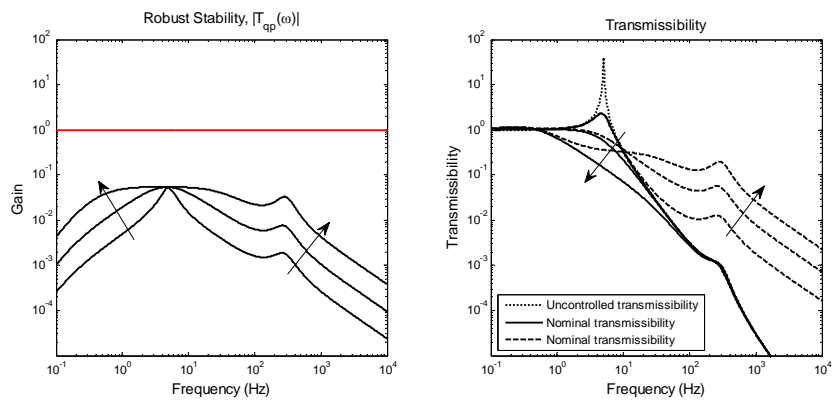


**Figure 37** Robust stability and robust performance plot of *system 3* using gain  $k = 4000, 16\ 000, 64\ 000$  (arrows indicate the direction of increasing gain)

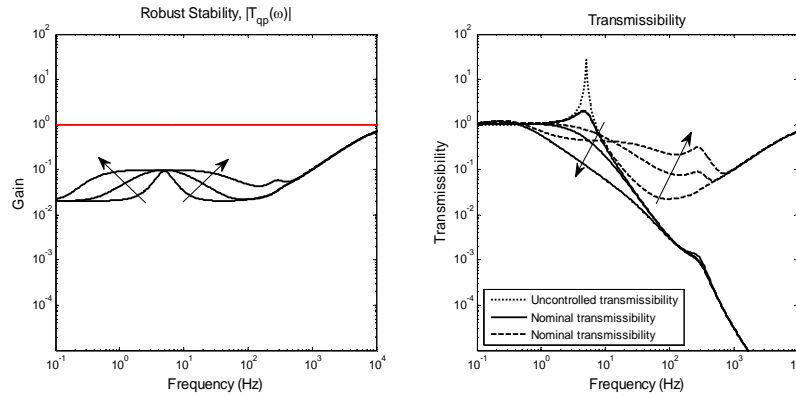


**Figure 38** Robust stability and robust performance plot of *system 4* using gain  $k = 25\ 000, 100\ 000, 400\ 000$  (arrows indicate the direction of increasing gain)

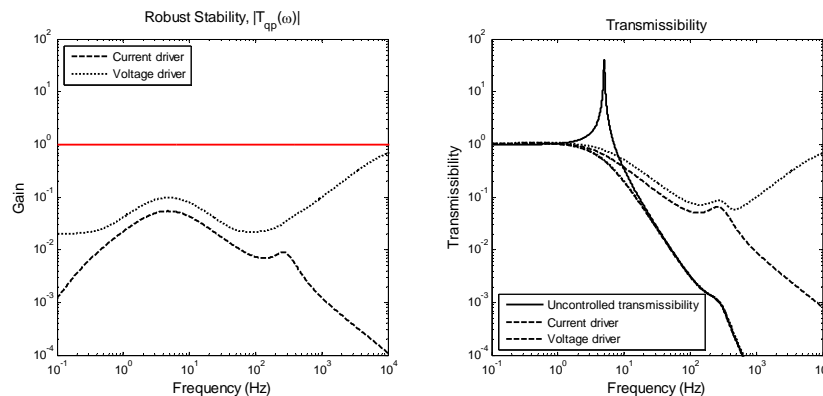


**Figure 39** Robust stability and robust performance plot of the *system 3* and *system 4*

Figures 37 and 38 show the robust stability plot and the nominal and robust transmissibility of the *system 3* and *system 4* using different controller gains. The arrows indicate the direction of gain increasing. The trend of robust stability and robust performance is similar to the soft-actuator case that is the system is still stable when the controller gain is increased. A better nominal transmissibility is achieved when the controller gain is increased; however, the robust performance deteriorates when the controller gain is increased.

Suppose the damping ratio of the first resonant frequency equal to  $\zeta = 1$  is required for each system. Setting the controller gain  $g = -h = -16\,700$  A/(m/s) for *system 3* and  $g = -h = -95\,800$  V/(m/s) for *system 4*. Figure 39 shows a comparison of the robust stability and robust performance of the two systems that use different kinds of driver. The nominal transmissibilities are similar, but the robust performance of the system that uses the current driver is better than that of the system that uses a voltage driver.

Clearly, to add external damper parallel an actuator can improve the stability characteristic of the controlled system and allow us to use a higher controller gain to achieve a better performance. In addition, to avoid dealing with the uncertainty in the electrical domain, the current driver should be used.

## 6. Summary

In this report, a two-port model has been used to describe the behaviour of three types of actuator namely electromagnetic, magnetostrictive and piezoelectric actuators. The constitutive equation of each actuator have been derived and presented in the form of two-port model.

To identify the parameters of the actuator, the relative velocity can be approximated by the absolute velocity of the moving part if the mass ratio between the moving mass and actuator case mass is small. An external mass can be added to the actuator case to ensure this condition holds. As a result, the mechanical impedance can be approximated by a single degree-of-freedom model.

The actuator parameters have been identified with no external load and the experimental results show that the constitutive equations predict the experimental results in low frequency range. The frequency response error between the model and the experiment is treated as an unstructured uncertainty.

In system design, there are many choices of actuator that are available. In order to achieve a satisfactory performance and acceptable cost, an actuator selection criteria

should be used. In this report, the force-displacement property, modulus squared value of blocked force per unit electrical power input, the modulus squared value of the free displacement per unit electrical power input, and maximum efficiency of each actuator has been studied. The electromagnetic actuator can generate a large displacement but low force. Conversely, a magnetostrictive actuator and a piezoelectric stack actuator can generate a large force but small displacement. In terms of the square of modulus of the free displacement per unit input electrical power, the electromagnetic actuator can generate the largest displacement with the smallest power consumption. However, in terms of the square of the modulus of the blocked force per unit input electrical power, the piezoelectric stack actuator is most efficient at low frequency but decreases with frequency and the magnetostrictive actuator maintains a good efficiency in all frequency ranges. In the matched load condition, the maximum efficiency of the electromagnetic actuator is roughly constant with frequency. The maximum efficiency of the magnetostrictive actuator increases with frequency. Conversely, the maximum efficiency of the piezoelectric stack actuator decreases with frequency. The study suggests that an electromagnetic actuator is suitable for a system that requires a large displacement but low force, a piezoelectric stack actuator is suitable for a system that operates in the low frequency range and requires a large force but small displacement, and a magnetostrictive actuator is suitable for the system that operates in the high frequency range and requires a large force but small displacement.

In section 5, the application of actuators to an active vibration isolation system has been demonstrated and the effect of uncertainty due to identification error has been studied. The study shows that a good isolation performance can be achieved by using a sky-hook-damper controller in both the soft-actuator and the stiff-actuator cases. The uncertainty in the actuator can reduce the gain margin of the system and can cause a deterioration in the performance (transmissibility) of the system. In the stiff-actuator case, adding an external damper parallel to the actuator can improve the gain margin of the system. The robust performance of the system can be improved in both cases by using a current driver. It should be noted that the conclusions are based on

the sky-hook damper type of controller. If another more sophisticated controller is employed, the use of a voltage driver might not be disadvantageous.

## 7. References

- [1] Brennan, M.J., Garcia-Bonito, J., Elliott, S.J., David, A. and Pinnington, R.J., (1999), *Experimental investigation of different actuator technologies for active vibration control*, Smart Structures and Materials, Vol.8, 145-53
- [2] Goldfarb, M.; Celanovic, N., (1997), *Modeling piezoelectric stack actuator for control of micromanipulations on micromanipulation*, Control System Magazine, IEEE, Vol.17, 69-76
- [3] Adriaens, H.J.M.T.S.; De Koning, W.L.; Banning, R., (2000), *Modeling piezoelectric actuators*, IEEE/ASME Transactions on mechatronic, Vol.5, 331 - 341
- [4] Dapino, M.J.; Smith, R.C.; Flatau, A.B.; (2000), *Structural magnetic strain model for magnetostrictive transducers*, IEEE Transactions on magnetics, Vol.36, 545 - 556
- [5] Zhou, K., Doyle, J.C. (1977), *Essentials of robust control*, New Jersey, Prentice Hall
- [6] Hunt, F.V., (1982) *Electro-Acoustics, the analysis of Transduction and its historical back ground*, New York, American Institute of physics.
- [7] Smith, R.C., (1997), *A nonlinear model-based control method for magnetostrictive actuators*, Proceedings of the 36th IEEE Conference on Decision and Control, Vol.4, 3715 – 3720.
- [8] Jackson, H.W., (1959), *Introduction to Electronic Circuits*, New Jersey, Prentice-Hall
- [9] Boyd, S., El Ghaoui, L., Feron, E., and Balakrishnan, V., (1994), *Linear Matrix Inequalities in System and Control Theory*, Studies in Applied Mathematics, SIAM, Philadelphia, Pennsylvania, Vol. 15.
- [10] Abu-Hanieh, A., (2003), *Active Isolation and Damping of Vibrations via Stewart Platform*, Ph.D. Thesis, ULB university.